BILINGUAL PUBLISHING CO.
Pioneer of Global Academics Since 1984

02

Non-Metallic Material Science

Volume 2 | Issue 2 | 2020 October | ISSN 2661-3301 (Online)

BILINGUAL
PUBLISHING CO.
Pioneer of Global Academics Since 1984

Editor-in-Chief

Editorial Board Members

Volume 2 Issue 2 • October 2020 • ISSN 2661-3301 (Online)

Non-Metallic Material Science

BILINGUAL PUBLISHING CO.
Pioneer of Global Academics Since 1984

BILINGUAL PUBLISHING CO.
Pioneer of Global Academics Since 1984

Volume 2 | Issue 2 | October 2020 | Page1-27
Non-Metallic Material Science

Contents

ARTICLE

REVIEW

BILINGUAL PUBLISHING CO.
Pioneer of Global Academics Since 1984

Non-Metallic Material Science
https://ojs.bilpublishing.com/index.php/nmms

ARTICLE

Development of Superhydrophobic Polyester (*Polyethylene terephthalate*) Fabric for Multiple Applications

Subhas Ghosh* **Roopkatha Pallye**

College of Engineering and Technology, Eastern Michigan University, Ypsilanti, Michigan, USA

ARTICLE INFO

Article history
Received: 6 May 2020
Accepted: 25 May 2020
Published Online: 30 October 2020

Keywords:
Polyester fabric
Contact Angle
Fluoro silane
Super hydrophobic
Stain repellant

ABSTRACT

This study intended to develop a healthy and environmentally friendly super-hydrophobic PET polyester textile fabric using a specific Fluoro Silane finish (SHF). A novel SHF was prepared and applied on a polyester fabric using a pad-dry-cure method. The finished fabric was evaluated for the degree of hydrophobicity, durability and stain repellence. The finished fabric exhibited static water contact angle greater than 170o and received 90 AATCC (4 ISO) rating that is recognized as super-hydrophobicity and this property was maintained even after a 50,000-cycle abrasion test. FTIR analysis identified the characteristic peaks related to Si-O-Si and C-F asymmetric stretching bands of the finish on the fabric indicating a robust attachment on the fabric. Finished fabric did not show any change in appearance or tactile characteristics of the fabric.

1. Introduction

Super-hydrophobic fabric technology was evolved from biomimetic technology. This was derived from the lotus leaf phenomenon as researched by many scientists. The term "Super-hydrophobic" is related to extremely high-water repellency of a substrate. When the static water contact angle θ is greater than 150°, the surface is super-hydrophobic [1]. Under such condition, the water drop forms a spherical shape achieving minimum surface area because of the cohesive forces between the water molecules. As the water drops fall on the surface, they effortlessly roll off the surface without wetting it at all. Because of very low surface energy of the super-hydrophobic surface, loosely held dirt and soils get easily attached to the rolling drops and are removed. The lotus leaf is one of the best-known natural super hydrophobic surfaces, that effectively removes mud, as water drops flow over the surface. A Nano-level hydrophobic natural wax crystal was found to be present on the top of the micro bumps on a lotus leaf, which makes the lotus leaf a self-cleaning as well as a strong hydrophobic surface [2]. There are several techniques that had been used by many researchers to produce super-hydrophobic textiles. Kawai and H. Nagata [3] had used soft lithography, X-Ray lithography, electron beam lithography, Nano sphere lithography and photolithography to develop super hydrophobic surfaces. Zhang et al [4] and Chen et al [5]

**Corresponding Author:*
Subhas Ghosh,
College of Engineering and Technology, Eastern Michigan University, Ypsilanti, Michigan, USA;
Email: sghosh@emich.edu

 DOI: https://doi.org/10.30564/omms.v2i2.1862

used the same technique by creating silicon nano-pillar arrays. A Phase separation technique was reported to be used for the preparation of super- hydrophobic surfaces. Polizos et al [6] obtained a hierarchical porous structure through interconnection of different dimension of pores. They used PEG Polyethylene glycol (PEG) and PDMS in 1:1 ratio in the phase separation to create a surface that had a water contact angle of 160°. Bao et al [7] used chemical vapor deposition method, where a substrate was created in the form of non-volatile film using gaseous reactants of metal oxide nanoparticles like ZnO, Al_2O_3 and Fe_3O_4 etc. that produced super hydrophobic fabric surfaces. Several researchers used sol-gel and other chemical to produce super-hydrophobic surfaces. Sahoo and Kandasubramanian [8] used organic, inorganic materials and metal alkoxides for sol-gel techniques. Hufnagel's et al. [9] produced super-hydrophobic cotton fabric using silica particles. They reported WCA was 155°. Ivanova and others [10] fabricated super-hydrophobic cotton fabric by altering the fabric structure using fluoro silane (Fs) material. Xue et al [11] used amino and epoxy functionalized silica nanoparticles along with stearic acid and 1H,1H,2H,2H-perfluorodecyl-trichlorosilane on cotton fabric to create super-hydrophobic characteristics and they claimed to achieve 170^0 WCA (Water Contact Angle). Meng et al., [12] Das and De, Meng et al. [13] used long chain fluorinated compounds on cotton fabric to create super-hydrophobic characteristics. All these methods produced various degrees of Super hydrophobicity on textile substrates; but the cost of production for commercially viable products having desired durability, quality and least environmental harm, still impedes mass production of such products.

In this investigation a Super-Hydrophobic and stain repellant polyester fabric was developed by synthesizing a superhydrophobic finish using a single fluoro-silane compound and applying it on the textile substrate using simple textile wet processing method. Since some fluorine compounds have been reported to have adverse effect on health this Fluorosilane was carefully selected so that it has no harmful effect to human health and environment. The US HMIS and NFPA agencies [14] rated the chosen Fluorosilane as 0 health hazard and 0 physical hazard. Fluoro silane was used in this investigation because the fluorinated methyl groups are less reactive and possess very low surface energy due to the presence of strong C-F bond than normal hydrophobic -CH_3 groups, providing very high hydrophobicity and stain repellency with creating no environmental issues.

2. Experimental Methods

Material: A 100%-woven polyester (PET) dyed fabric was used. The fabric was a plain weave having a weight of 6.71 0z/yd^2 and woven from False Twist Textured yarns. The construction was 48 x 48, ends x picks per inch.

Chemicals: Reagent-grade solvent butanol, disodium hydrogen phosphate, 72% sulfuric acid solution, titanium tetra butoxide, and anhydrous NaOH pellets were obtained from Sigma Aldrich. FS (FDTES) was obtained from Matrix Scientific. All chemicals were used without further purification.

PET fabric pre-treatment: In order to generate more attaching functional groups on the polyethylene terephthalate chains so that the super-hydrophobic finish is more durable when applied on the fabric, an alkaline partial hydrolysis was conducted on the specimen fabric. Polyester affected by alkali depending on their ionic character. Only the outer surface of polyester gets affected by ionizable alkali like caustic soda NaOH. De-esterification of polyester results in the formation of free-functional groups at the fiber surface as seen in Figure 1, which are terminal hydroxyl and carboxyl end groups (14). After washing the fabric in a nonionic detergent at 50^0 C , de-esterification was performed at 85°C in a water bath containing 6% sodium hydroxide, for 20 min, in the presence of 1% titanium tetra butoxide as an initiator. The % NaOH, temperature and de-esterification time were determined using a designed experiment so that enough generation functional groups occur without losing any significant strength of the Fabric. The de-esterified sample was rinsed in mild H_2SO_4 solution to neutralize the fabric.

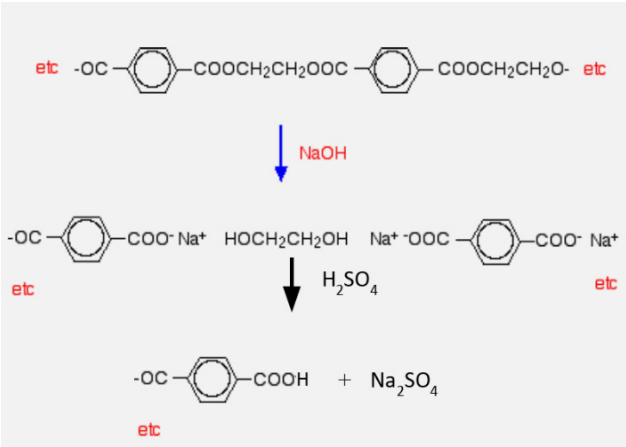

Figure 1. illustrate the PET polyester de-esterification process

Preparation of the Superhydrophobic (SHF) finish and Application: A pre-determined amount of

DOI: https://doi.org/10.30564/omms.v2i2.1862

Perfluorodecyltriethoxysilane (FDTES) was added to the reagent-grade solvent butanol and stirred continuously at room temperature at 350 RPM. A small amount of the catalyst, disodium hydrogen phosphate, was added to facilitate the addition of the finish to the prepared polyester specimens. A few drops of sulfuric acid were added slowly to the mixture while stirring to maintain the very low pH of 2, to control the condensation reaction. The required amount of additional butanol was added and stirring was continued. The solution was stirred continuously for one hour and was placed in the refrigerator for 24 hours prior to application. Care was taken to evade rapid condensation reaction and precipitation by carefully monitoring pH and condensation time. The superhydrophobic finish was synthesized and then applied to the de-esterified fabric specimen using a traditional dip pad cure method. The additional finish was force sprayed onto the fabric surface prior to the fabric entering the padding mangle. This facilitated the finish to migrate into the interstices of the woven structure evenly. The fabric was dried at 60 ^{o}C for 15 minutes and then cured at 165 +/- 5 ^{o}C for 15 minutes for complete attachment of the finish. These conditions were previously optimized and verified in the preliminary research.

Spectroscopic analysis by FTIR: A PerkinElmer Fourier-transform infrared (FTIR) spectrophotometer was used for spectroscopic analysis of the prepared samples. This method was used to examine the effects of de-esterification on the PET fabric and application of SHF finish on the fabric.

Determination of Water Contact Angle (WCA): WCA was determined using a Static Contact Angle method. A contact angle measurement device First Ten Angstrom (FTA-200) was used for measuring static contact angle. Images for contact angle measurement were captured using an Amscope MU853B 14MP high-speed digital camera, attached to the device set up. Five readings were taken on different areas of the same sample and were analyzed by the computer plugin LBADSA available with the open-sourced JAVA application ImageJ. In the LBADSA method, the theoretical profile of the drop is not fitted to a certain drop contour but is rather optimized according to an image energy approach. It is based on the perturbation solution of the axisymmetric Laplace equation. During the fitting process, complete pixel information is used. The use of this global model results in exactly accurate contact angles. This approach chiefly has an edge over other methods when a precise accurate contour detection is difficult because of un-sharp or noisy boundaries of textile fabrics [15].

Water repellency spray test: Superhydrophilicity of the treated fabric was evaluated for water repellency by spray test according to AATCC TM22 (ISO 4920). The test samples were rated according the rating chart provided by AATCC where a value 100 is given to the test specimen when no sticking or wetting occur on upper surface and a 0 value is given for complete wetting of upper and lower surfaces after the water spray. A substrate is recognized as superhydrophobic when a rating of 80 and higher is obtained. The fabric surface is described as wet at spray point only at 80 ratting. The results obtained from this test method are largely dependent on water repellency of the yarns, fibers, and finish on the fabric and not upon the construction of the fabric.

SHF finish durability test of the treated fabric: The durability of the finish on fabric was measured by abrasion resistance test using 50,000 cycles by ASTM method D4966-12 on a Martindale abrasion tester. Before and after abrasion, the specimens' weight losses and contact angles were measured. In addition, spectroscopic data was obtained to evaluate the effect of abrasion on finish attachment.

Stain Repellency Evaluation: Stain repellency was tested against mayonnaise, jam, and hot sauce on the fabric surface separately, and the specimens were left for 15 minutes after application of the staining substances. Then, the fabric was rinsed with normal tap water and dried. The post-washing samples were rated for stain using AATCC - 300 stain visibility chart where 5 in no stain and 0 is maximum staining of the specimens.

3. Results and Discussion

Free functional end groups were created by breaking the esterification links of PET chains under controlled de-esterification conditions. During the de-esterification process, few long chains of the fiber polymers break down and produce larger numbers of free functional end groups such as OH- and COO- groups. As seen in Figures 2 and 3 a broad band associated with OH groups are Present at 2930 cm^{-1} .

Furthermore C=O band of ester linkages near 1745 cm^{-1} increased because of the de-esterification of PET chains and continued to increase with the NaOH concentration. We used 6% alkaline concentration for 15 minutes in the de-esterification process that provided enough functional groups on the PET chains. This sample was used for the application of the SHF finish because there was no significant change in the fabric strength as measured before (80 lbf) and after (81lbf) de-esterification.

 DOI: https://doi.org/10.30564/omms.v2i2.1862

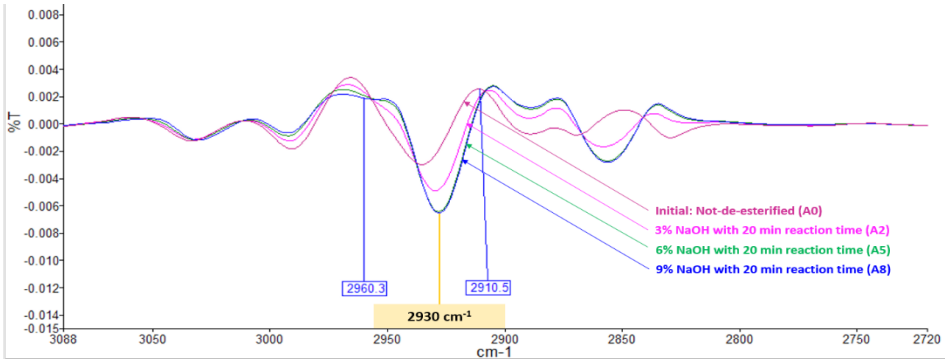

Figure 2. Second derivative transformed FTIR scans for de-esterified PET samples around the OH- bands

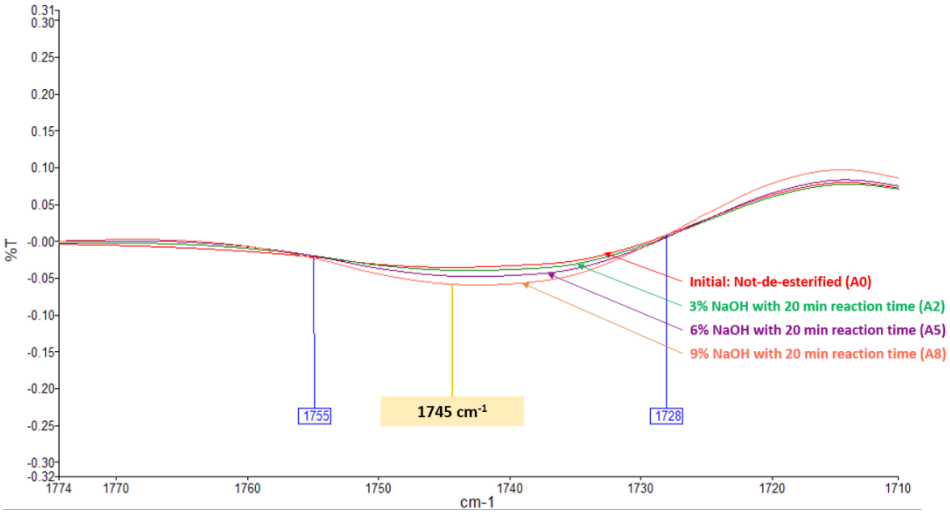

Figure 3. Second derivative transformed FTIR scans for de-esterified PET samples around the COOH- bands

De-esterified PET samples were treated with Fluorosilane finish and cured at an elevated temperature near 165° C resulting condensation reactions between the Fluorosilane finish and ends groups generated on the PET fabric samples thus, binding the finish on the fabric surface as illustrated in Figure 4 describing the attachment mechanism.

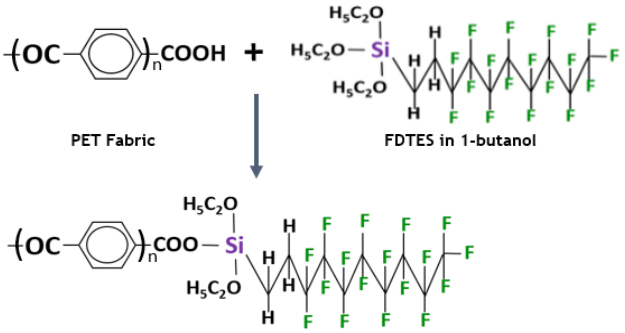

Figure 4. Shows the attachment scheme of the Fluorosilane finish on the PET fabric surface

The FTIR analysis of the Fluorosilane treated fabric sample provided a good indication about the attachment of the finish. As illustrated in Figure 5, the spectra of the treated fabric shows the peaks at 852cm^{-1} -1094 cm^{-1} that are related to asymmetric stretching of Si-O-Si bonds and the picks appeared at 744.5 cm^{-1} and 948.88 cm^{-1} are assigned to the C-F bonds (16) arising from the SHF finish on the fabric. These evidences suggest that applied finish is attached to the fabric structure. Water Contact Angle (WCA) measured on the SHF finished specimen using LBADSA method, exhibited 178.2° WCA; the same fabric specimen was subjected to 50,000 cycles of abrasion that provided 170.8° WCA. These results reveal the strong superhydrophobic characteristic property of the fabric and the durability of its super-hydrophobicity.

DOI: https://doi.org/10.30564/omms.v2i2.1862

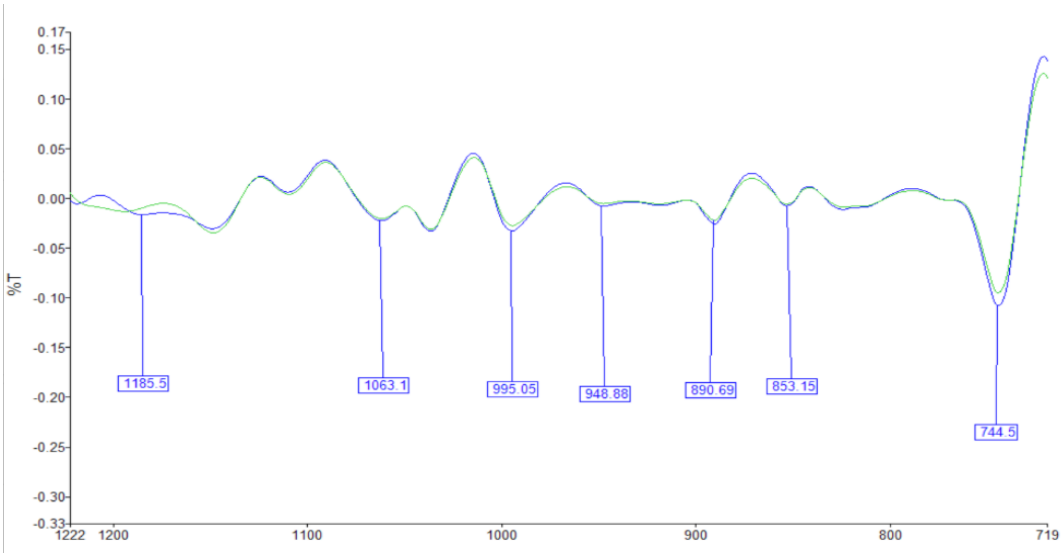

Figure 5. FTIR Spectra of SHF finished polyester fabric in regions Si-O-Si and C-F peaks

Water repellency spray test was performed on the SHF finish treated samples using AATCC TM22 (ISO 4920) that yielded a rating of 90 according to the AATC rating chart. It was observed that the treated sample exhibited a slight random sticking of water on the upper surface, which was removed by shaking the fabric sample, and there was no water mark at all on the lower side of the sample but original untreated sample was completely wet on both upper and lower surface after the water spray, obtaining the lowest rating of 0. Usually a rating of 80 rating is considered in the industry as a requirement for a superhydrophobic fabric. A test sample is illustrated in figure 6.

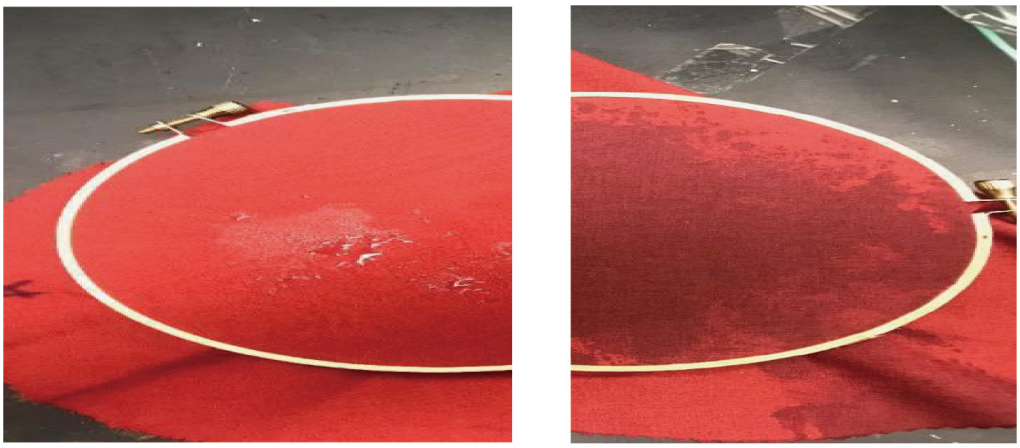

Figure 6. FS-treated sample and original untreated sample after AATCC TM22 water spray test

A stain repellency test was conducted by using the AATCC 130 method, and the rating was given according to the Stain Release Replica grade (AATCC 130). The original untreated and FS-treated samples were stained with mayonnaise, jam, and hot sauce. The samples were left for 30 minutes after application on the surface, after which the applied staining agents were wiped out by a dry tissue paper. As seen in Figure 7, there was no stain or any mark on the SHF-treated superhydrophobic specimen, however a clear stain was noticed on the original untreated sample. According to the AATCC 130 stain release replica grading chart, the SHF-treated sample received a grade of 5, which indicates there was no stain on it. Whereas the untreated fabric received a 0 rating, because there was no change in the stain created by the staining agents.

 DOI: https://doi.org/10.30564/omms.v2i2.1862

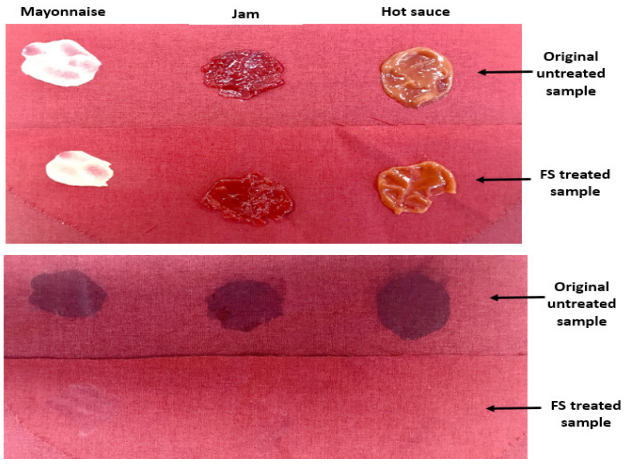

Figure 7B. original untreated and SHF-treated samples after wiping out with a tissue

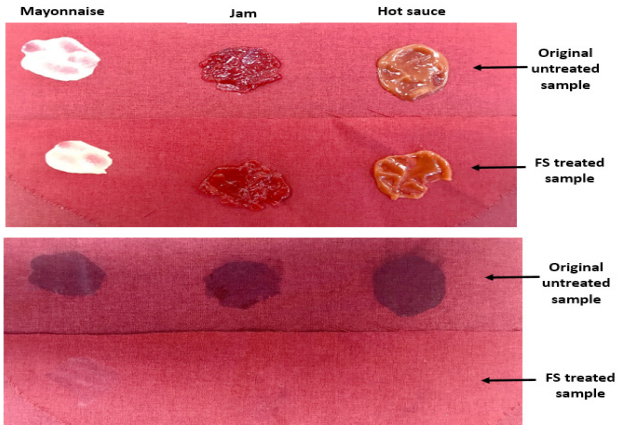

Figure 7A. The original untreated and SHF-treated samples after the applied staining agents

The SHF finished fabric was tested against coffee heated to the temperature at which it is generally served at coffee shops (60 °C), Coke at 10 °C, which is the normal temperature inside refrigerators in stores, and red wine at room temperature (25 °C). After these liquids were poured on to the fabric, they were observed to form spherical droplets as shown in Figure 8. After 10 minutes, when the fabric was tilted, and the liquid drops were observed to roll out without wetting or staining the fabric. When the droplets were standing on the fabric, the contact angle (CA) values were measured to be above 140°, which is in the range of superhydrophobic character as given in Figure 8. Furthermore, vegetable cooking oil drops were placed on the fabric and was watched for one hour. The fabric did not absorb the oil at all, and after 1 hour, the oil drops were easily removed by wiping with dry tissue paper, without any staining or absorption of the oil in the fabric.

Figure 8. illustrating liquid drops on the SHF finish treated polyester fabric surface

4. Conclusions

This study developed a Super-hydrophobic PET polyester fabric using a specific SHF finish. The treated fabric did not show any changes in the surface appearance and in tactile property. Experimental data showed that super-hydrophobic property of the fabric was maintained even after undergoing 50,000 abrasion cycles. Different kinds of liquids including tea, coffee and wine, formed spherical droplets on the fabric surface and rolled off the fabric surface without wetting or adhering to the fabric. The treated fabric had a water contact angle >=170°, even after 50,000 abrasion cycles, implying the finish was durable. Water Repellency Spray test provided 90 (AATCC Rating) which is the commonly accepted value by industry for a super-hydrophobic fabric. No residue and stain were observed on the wiped fabric during the stain-repellency test against mayonnaise, jam and hot sauce. FTIR data identified the presence of SHF finish on both the treated fabric before and after abrasion. It is concluded from the experimental data that the SHF finish used on the polyester fabric provided a durable super hydrophobic characteristic. A unique feature of this finish and the method for the super-hydrophobic fabric is its suitability for the commercial process and reasonable cost. Super-hydrophobic finished fabrics have several applications including apparel, automotive interior and hood for the convertible automobiles, army clothing, medical textiles, military clothing, furniture, outdoor furniture and other.

References

[1] Zhao H., Ras H.A. Definitions for Hydrophilicity, Hydrophobicity, and Superhydrophobicity: Getting the Basics Right. The Journal of Physical Chemistry Letters, 2014: 686-688.

[2] Barthlott W., Neinhuis C. Purity of the sacred lotus, or escape from contamination in biological surfaces. Planta, 1997: 1-8.

[3] Kawai A., Nagata H. Wetting Behavior of Liquid on Geometrical Rough formed by Photolithography,

DOI: https://doi.org/10.30564/omms.v2i2.1862

Journal of Applied Physics, 1994.

[4] Zhang X., Zhang J., Ren Z., Li X., Zhang X., Difu Z., Wang T., Tian T.,Yang B. Modulating two-dimensional non-close-packed colloidal crystal arrays by deformable soft lithography. Langmuir, 2009.

[5] Chen J. K, Qui J. Q., Fan S. K., Kuo S. W., Ko F. H., Chih- Wei C., Chang F. C. Using Colloid Lithography to fabricate silicon nanopillar arrays on silicon substrates. Journal of Colloid and Interface Science, 2012.

[6] Polizos G., Tuncer E., Qiu X., Aytug T., Michelle Kidder K., Messman J. M, Sauers I. From Hydrophobic to Superhydrophobic and Super hydrophilic Siloxanes by Thermal Treatment. Langmuir, 2011.

[7] Bao X.M., Cui J.F., Sun H.X., Liang W.D. Zhu Z.Q., An J., Yang B.P., La P.Q., Li A. Facile preparation of super-hydrophobic surfaces based on metal oxide nanoparticles. Applied Surface Science, 2014: 473-480.

[8] Sahoo B.N., Kandasubramanian B. Recent progress in fabrication and characterization of hierarchical biomimetic super-hydrophobic, Royal Society of Chemistry Advances, 2014.

[9] Hoofnagle's H.F.,Wu D.,With G.D., Ming W. Biomimetic Superhydrophobic and Highly Oleophobic Cotton Textiles, Langmuir, 2007.

[10] Ivanova N.A., Lavretsky A.K., Ivanova N.A., Zaretskaya A.K. Imparting Waterproof Properties to Cotton Surface. Protection of Metals and Physical Chemistry of Surfaces, 2011: 369-371.

[11] Xu C.H., Jia S.T., Zhang J., Tian L.Q. Super-hydrophobic surfaces on cotton textiles by complex coating of silica nanoparticles and hydrophobization, Thin Solid Films, 2009.

[12] Das I., De G. Zirconium based super-hydrophobic coatings on cotton fabrics exhibiting excellent durability for versatile use, Scientific Reports, 2015: 1-11.

[13] Meng S., Ye Y., Mansouri J.,Chen V. Crystallization behavior of salts during membrane distillation with hydrophobic and super-hydrophobic capillary membranes. Journal of Membrane Science, 2015: 165-176.

[14] Bendak, S. M., & Marsafi, E. Effects of chemical modifications on polyester fibers. Journal of Islamic Academy of Sciences, 1991, 4(4): 275-284.

[15] Río, O. I., Kwok, D.Y., Wu, J. R., Alvarez, J. M., Neumann, A.W. Contact angle measurements by axisymmetric drop shape analysis and an automated polynomial fit program. Colloids and Surfaces A: Physicochemical and Engineering Aspects, 1998, 143(2-3): 197-210.

[16] Brassard, J. D, Sarkar D. K., Perron, J. Fluorine based superhydrophobic coatings. Applied Sciences, 2012, 2(2): 453-464.

 DOI: https://doi.org/10.30564/omms.v2i2.1862

BILINGUAL PUBLISHING CO.
Pioneer of Global Academics Since 1984

Non-Metallic Material Science
https://ojs.bilpublishing.com/index.php/nmms

ARTICLE

Synthesis and Characterization of Trivalent Al Substituted Zinc Ferrite using Ethylene Diamine (EDA) as Ligand

Soumya Mukherjee*

Department of Metallurgical Engineering, Kazi NazrulUniversity, PO Kalla More, Asansol, 713340, India

ARTICLE INFO

Article history
Received: 6 May 2020
Accepted: 25 May 2020
Published Online: 30 October 2020

Keywords:
Al substituted Zinc ferrite
Ethylene Diamine
Thermal analysis
Phase analysis
Strain analysis

ABSTRACT

Nano domain Al substituted Zinc ferrite was prepared by chemical route using Ethylene Diamine as ligand. High purity precursors nitrate salts of Zinc, $Fe^{(3+)}$, $Al^{(3+)}$ were utilized along with citric acid which acts as both fuel and complexing agent. Two different molar ratios of $Zn^{(2+)}$:(Fe^{3+}):$Al^{(3+)}$ is 1:1.5:0.5 and 1:1.25:0.75. After ensuring proper mix of the solution Ethylene diamine was added dropwise to form a gel like mass with proper pH control. Before annealing, thermal analysis was carried to determine the crystallization/phase transition zone. Drying was carried in several stages. Initially, gel like mass was obtained after drying at 40°C while pH was about 7. Drying of gel was carried in oil bath at about 90°C and powdered mass obtained was grinded followed by auto combustion at 150°C for 60 minutes before annealing at 150°C, 350°C, 650°C, 950°C for 2 hours to ensure the phase formation. Crystallite size, lattice strain and lattice parameters were studied from XRD analysis.

1. Introduction

Due to presence of unique properties ferrites becomes a material of interest for the last few recent years. Ferrites are noted to have potential applications as storage for electronic, microwave for high resistivity property and also for magnetic applications under high frequency. Ferrites are also noted for application in memory devices, telecommunication devices, ferrofluids, transformer cores, recorders and others. In recent times, spinel ferrites are also noted for applications in biomedical devices, waste water treatment and catalysis of compounds. [1-3] Spinel ferrites can be three types normal spinel, inverse spinel and random spinel ferrite type. Spinel in general represented by AB_2O_4 where A is divalent metal and B trivalent metal ions respectively. A cations are having one eight of the tetrahedral holes occupied while B cations are having one half of octahedral holes occupied while A-O coordination is tetrahedral one while B-O coordination is octahedral one. The tetrahedral sites are occupied by divalent metal cations like Mg^{+2}, Co^{+2}, Zn^{+2}, Cd^{+2}, Cu^{+2} while octahedral sites are occupied by trivalent cations like Fe^{3+}, Dy^{3+}, Al^{3+}, Gd^{3+}, Eu^{3+} and others. [1] In case of inverse spinel, A site is occupied by trivalent cations and B site is occupied by both divalent and trivalent cations. In several cases of spinel ferrites, an intermediate degree of

**Corresponding Author:*
Soumya Mukherjee,
Department of Metallurgical Engineering, Kazi NazrulUniversity, PO Kalla More, Asansol, 713340, India;
Email: smmukherjee3@gmail.com

DOI: https://doi.org/10.30564/omms.v2i2.1863

inversion among cation site distribution occurs. Due to such inversion among cationic distribution both sites are found to be occupied by both divalent and trivalent cations. Spinel ferrites are ferrimagnetic ordering where magnetic moments of A and B site cations are all aligned parallel to each other leading to net magnetic moment. [4-6] Development of magnetic tunability depend on selection of cations and their distribution at A sites and B sites respectively. Since Zn^{+2} and Fe^{+3} ions can be distributed over both A and B sites, Zinc ferrite can be represented by $(Zn_{1-\delta}Fe_{\delta})[Zn_{\delta}Fe_{2-\delta}O_4]$ where portion occupied by round brackets indicate atom position at A sites where as those occupied by square brackets as B sites and δ is called the inversion parameter. The inversion parameter δ=0 for conventionally prepared spinel while the value can reach upto 0.22 for as quenched samples. Nano spinel zinc ferrite exhibits mixed spinel category where the degree of inversion depends on the synthesis process. [6-10] In recent years spinel based oxides are noted to be effective for photocatalyst application specially in UV region. This particular oxide is noted to have some advantage over metal oxide semiconductors which are generally put to use for such applications. A particular case is for Titania as catalyst which is found to be difficult for removal from treated fluid flow thus limiting the application in major scale. Moreover, during catalysis reaction, small crystal size, high surface area of titania undergo some agglomeration thus inhibiting the application. Many industrial applications like alkylation reactions, methylation reactions, CO_2 reduction, alcohol decomposition, hydrogen peroxide decomposition and others are noted to be carried effectively by using spinel ferrite as potential catalyst. [11-17] Various routes have been carried for synthesis of ferrite nanoparticles like co-precipitation, sol-gel, micro-emulsion, ball milling, PVP capping as agent for synthesis, hydrothermal method and so on. [18-22]

In the present Al substituted Zinc ferrite was prepared using Ethylene diamine as ligand. Negligible research is carried till date on synthesis and characterization of Al substituted Zinc ferrite using the ligand as a novel chemical route via complexation reaction.

2. Experimental Method

In the present article AR grade high purity precursors of Zinc $^{2+}$, Al^{3+}, Fe^{3+} nitrates were utilized along with citric acid. 2 molar ratios of Zn^{2+}:Fe^{3+}:Al^{3+} having 1:1.5:0.5 and 1:1.25:0.75 were prepared while citric acid molar ratio was equal to the total molar ratio of metal salts. Citric acid plays the dual role of fuel and complex forming agent. Appropriate amount of nitrate salts were added to the beaker along with optimum amount of distilled water. By means of magnetic stirring saturated solution was prepared and citric acid was added. Ethylene diamine was added dropwise into the resultant solution under stirring conditions. With addition of ethylene diamine the solution becomes highly viscous gel like mass at pH of about 7. This transformation was carried at temperature of about 40°C. Gel was dried at 90°C in oil bath followed by grinding of dried gel in agate mortar pestle for autocombustion at 150°C for 60 minutes. Auto combustion reaction results in flappy blackish brown mass and it was made to undergo annealing at 150°C, 350°C, 650°C and 950°C for 2 hours to obtain the desired phase. A part of sample obtained after autocombustion was put for thermal analysis by DSC-TGA (Perkin Elmer, Diamond Pyris) to study crystallization/annealing zone. Phase analysis was carried by XRD (Rigaku, Ultima III) followed by lattice parameters and lattice strain calculation from XRD data.

3. Result and Discussion

3.1 Thermal Analysis

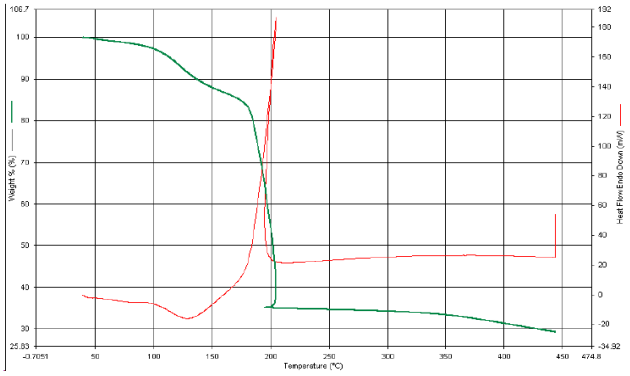

Figure 1. DSC-TGA of gel sample after auto combustion at 150°C having Al^{3+} 0.5 molar ratio using Ethylene diamine as ligand

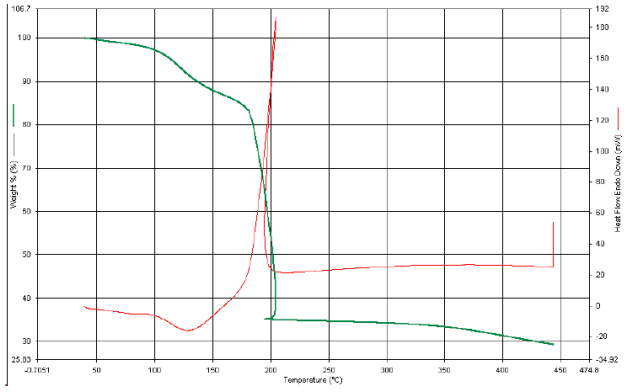

Figure 2. DSC-TGA of gel sample after auto combustion at 150°C having Al^{3+} 0.75 molar ratio using Ethylene diamine as ligand

From DSC-TGA analysis it is evident that drastic

weight loss occurs in two stages upto 200°C followed by flat weight changes. For both samples 1 &2, initial 10% weight change is observed till 140°C while 50% weight change is noted from 140 to 200°C with a sharp exothermic reaction noted at about 180°C. Weight losses are attributed to water of crystallization along with slight combustion reaction indicated while slight weight change is noted from 300°C to 400°C. The possible reaction at about 180°C would be the decomposition of complexing agent assisting the Al substituted Zinc ferrite formation. For both samples decomposition of complex initiates at about 150°C and stops at 200°C.

3.2 XRD Analysis

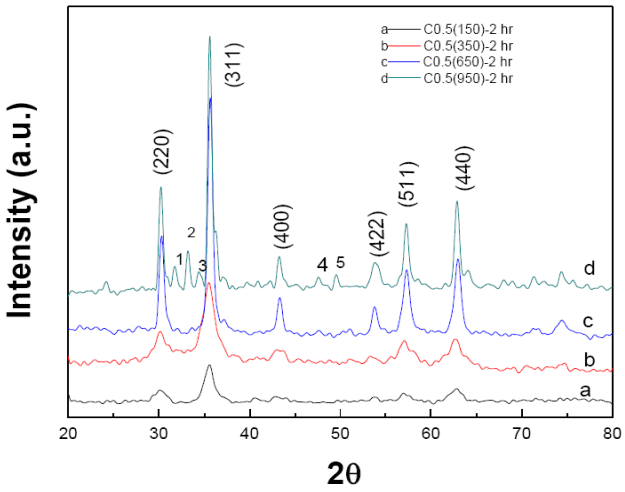

Figure 3. XRD plot of x=0.5 Al molar ratio substituted Zinc Ferrite at a) 150°C, b) 350°C, c) 650°C and d) 950°C for 2 hours using EDA as ligand

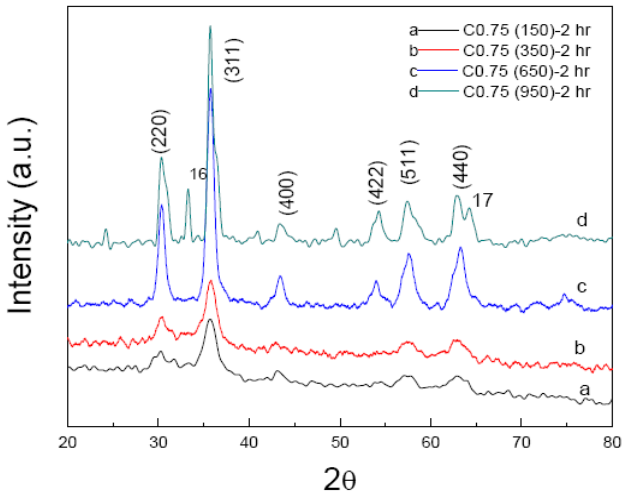

Figure 4. XRD plot of x=0.75 Al molar ratio substituted Zinc Ferrite at a) 150°C, b) 350°C, c) 650°C and d) 950°C for 2 hours using EDA as ligand

XRD analysis (Figure 3 & 4) exhibits crystallographic planes after annealing at 150°C, 350°C, 650°C and 950°C for 2 hours soaking period. At lower temperature having fixed soaking period, peaks noted are broad with humps indicating slight amorphous nature. With increase in temperature peak intensity rises indicating better crystallinity. Prominent peaks are noted along (22), (311), (400), (511) and (440) planes which have thermodynamic stability for growth. Crystallite size is estimated using scherrers formula and got compared with JCPDS card No 82-1048. Crystallite size is noted to be about 8.31nm, 5.45nm, 13.21nm and 16.29nm for x=0.5 mole Al^{3+} substitution at 150°C, 350°C, 650°C and 950°C for 2hours respectively. Increase in crystallite size is due to enhanced diffusion of atoms across grain boundaries due to thermal activation. All of the peaks got indexed with $ZnFe_{1.5}Al_{0.5}O_4$ (Figure 3) and with $ZnFe_{1.25}Al_{0.75}O_4$ (Figure 4) in the temperature range of 150°C to 650°C for 2 hours soaking. In case of $ZnFe_{1.5}Al_{0.5}O_4$ at higher temperature of 950°C minor amounts of Fe_2O_3 peaks are noted (peak indicated as 1,2,4,5) in Figure 3 while peak no 3 is for FeO as analyzed by XRD after verifying with JCPDS data card of respective individual elemental oxides of the synthesized compound. From Figure 4 it is noted that for higher mole fraction of Al substitution only Fe_2O_3 is formed for 2 small peaks (peak indicate as 16, 17) while no FeO is formed in this case. Similar to the case of x=0.5 mole fraction of Al^{3+} substitution, substitution with x=0.75 mole fraction also exhibits increase in crystallite size with temperature for fixed soaking period of 2 hours respectively. Crystallite size is noted to be about 6.33nm, 6.47nm, 10.50nm, 16.69nm for 150°C, 350°C, 650°C and 950°C respectively. For both case, strong crystalline peaks are noted with increase in temperature. Moreover, with higher Al substitution (x=0.75) for the same Ethylene diamine ligand having same soaking temperature and soaking period higher purity of the compound is noted in compare to lower Al substitution (x= 0.5). Using Williamson hall analysis crystallite size is estimated to be 3.38nm, 11.9nm, 20.8nm, 17.86nm for annealing at 150°C, 350°C, 650°C, 950°C for 2 hours with 0.5 molar Al^{3+} substitution. In case of 0.75 molar Al^{3+} substitutions for similar temperature and soaking condition crystallite size calculated using Williamson hall plot is observed to be 4.85nm, 15.38nm, 25.64nm and 66.67nm respectively.

DOI: https://doi.org/10.30564/omms.v2i2.1863

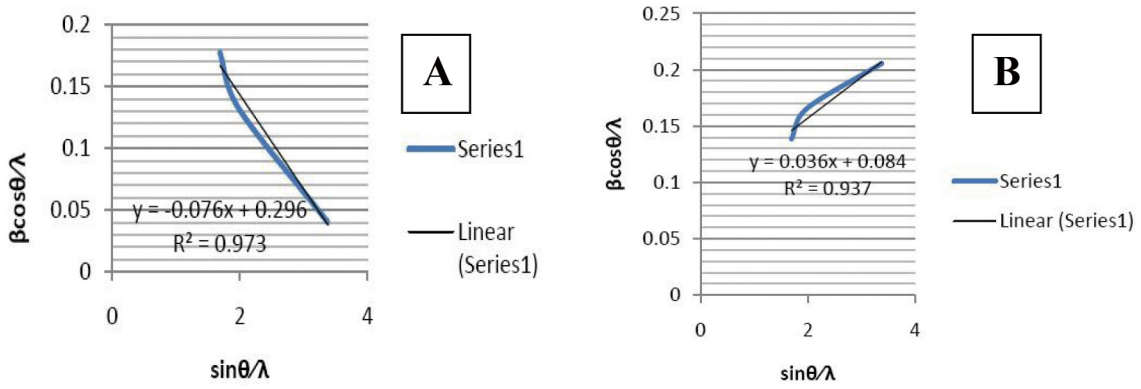

Figure 5. Plot of βCosθ/λ and Sinθ/λ for sample with x=0.5Al substitution using EDA as ligand at A) 150°C & B) 350°C for 2 hours

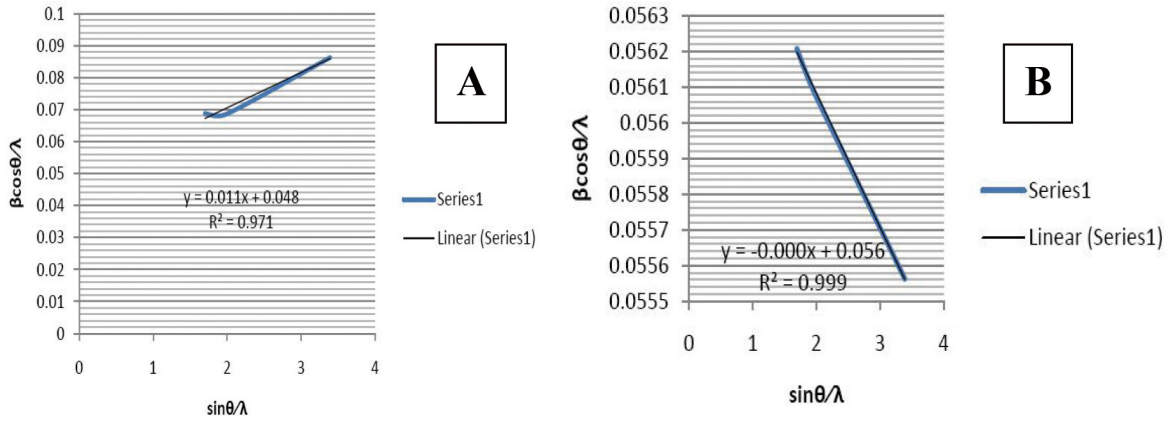

Figure 6. Plot of βCosθ/λ and Sinθ/λ for sample with x=0.5Al substitution using EDA as ligand at A) 650°C & B) 950°C for 2 hours

It is observed from the plot of βCosθ/λ Vs Sinθ/λ (Figure 5 & Figure 6) values of R^2 is close to unity. Thus the plot is close to linearity suggesting that the particle size would be towards monodispersive nature. These above plots indicate that the particle size does not represent scatter in observation or in other words narrow particle size distribution is possible.

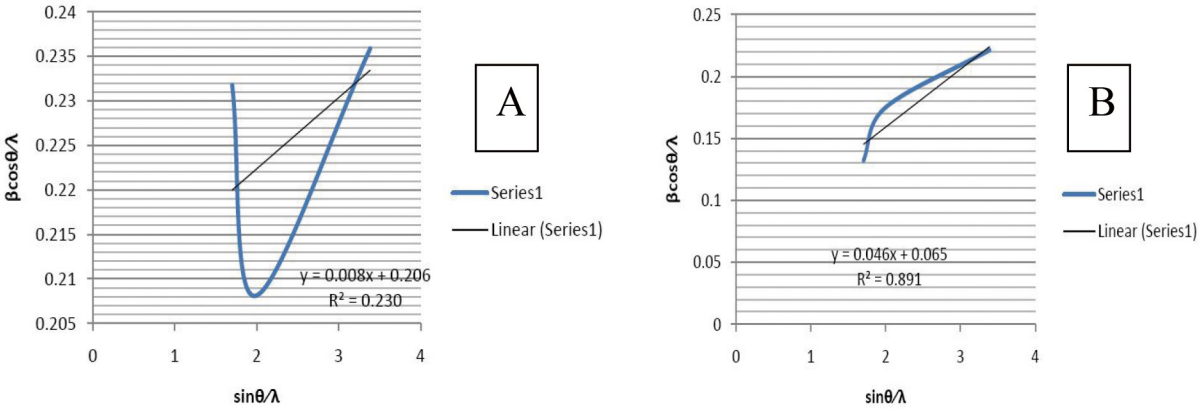

Figure 7. Plot of βCosθ/λ and Sinθ/λ for sample with x=0.75Al substitution using EDA as ligand at A) 150°C & B) 350°C for 2 hours

 DOI: https://doi.org/10.30564/omms.v2i2.1863

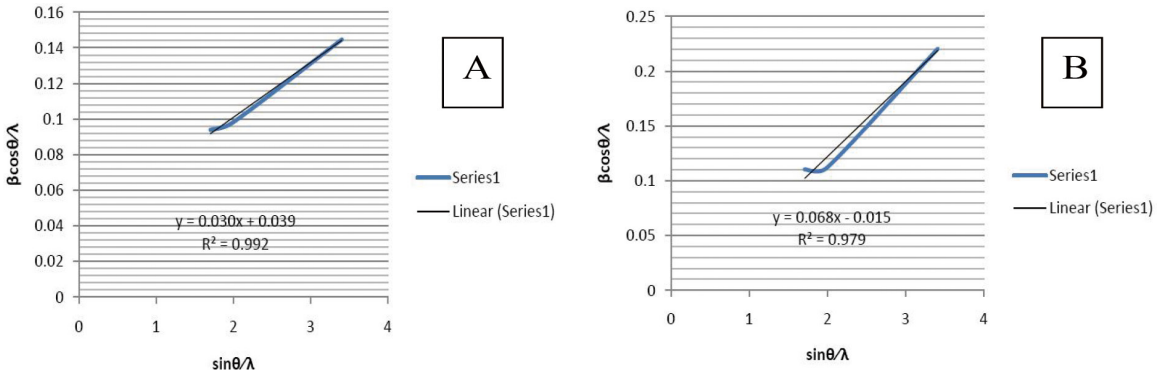

Figure 8. Plot of βCosθ/λ and Sinθ/λ for sample with x=0.75Al substitution using EDA as ligand at A) 650°C & B) 950°C for 2 hours

It is observed from the plot of βCosθ/λ Vs Sinθ/λ (Figure 7 & Figure 8) values of R^2 is close to unity but in one case the deviation is far away from unity. Observations of plot close to linearity suggest that the particle size would be towards monodispersive nature. One major deviation observed in linearity may be due to higher Al substitution in Zinc ferrite and size difference between Al^{3+} (0.53Å) and Fe^{3+} (0.64Å) ions. Higher proportion of Al^{3+} substitution may leads to prominent size distribution difference and strain effect on the matrix of the compound.

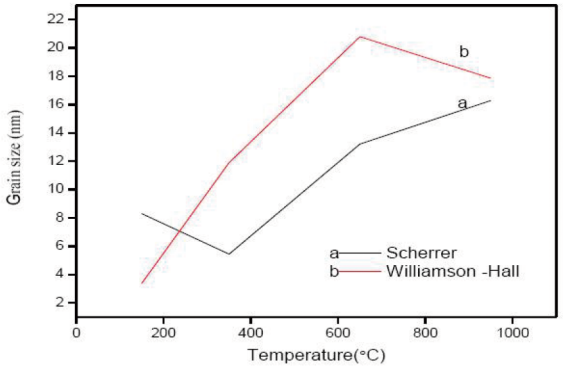

Figure 9. Variation of grain size Vs temperature for $ZnAl_{05}Fe_{1.5}O_4$ using EDA as ligand along with comparison of Scherrers and Williamson Hall data

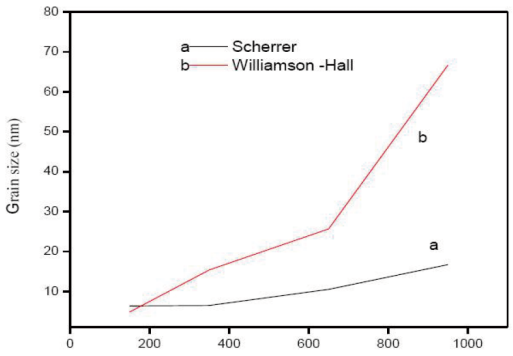

Figure 10. Variation of grain size Vs temperature for $ZnAl_{075}Fe_{1.25}O_4$ using EDA as ligand along with comparison of Scherrers and Williamson Hall data

Both Figure 9 & Figure 10 exhibits variation of grain size with temperature using EDA as ligand. Both higher and lower substitution of Al^{3+} exhibits almost same trend for both Scherrer and Williamson hall plot. The nature of graph is following the same trend which is noted for grain size growth with increase in temperature due to enhanced diffusion.

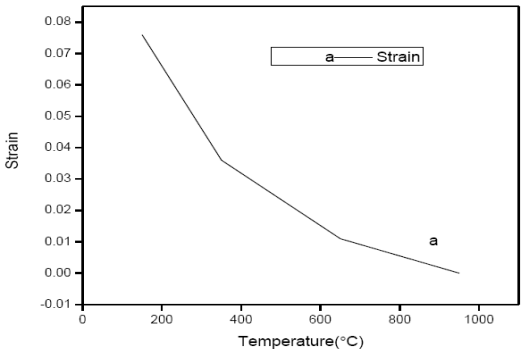

Figure 11. Variation of lattice strain for $ZnAl_{05}Fe_{1.5}O_4$ using EDA as ligand with temperature

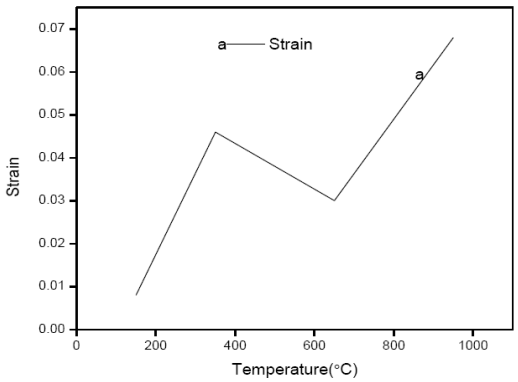

Figure 12. Variation of lattice strain for $ZnAl_{075}Fe_{1.25}O_4$ using EDA as ligand with temperature

Figure 11 & Figure 12 exhibits lattice strain variation for both Al substituted (x=0.5) and (x=0.75) mole fraction on Zn-ferrite matrix with annealing temperature for fixed soaking period of 2 hours. For x =.5 mole Al

DOI: https://doi.org/10.30564/omms.v2i2.1863

substituted Zinc ferrite strain decreases with temperature due to relaxation a general observation. But for x=0.75 mole Al substitution, lattice strain variation with temperature is irregular type and compare to previous case (Figure 7A) strain factor increases. The above result is in correspondence to XRD phase formation and R^2 value noted from βCosθ/λ and Sinθ/λ plot of samples synthesized and analysed by XRD at various temperature. The value of R^2 is quite regular with close to unity for all case for x=0.5 mole Al substitution but for higher substitution, the value is sporadic in one case while close to unity for other cases. The exact values of lattice strain for $ZnAl_{05}Fe_{1.5}O_4$ is about 0.076, 0.036, 0.011 and 0.02 respectively with increase in annealing temperatures 150°C, 350°C, 650°C and 950°C finally. Similarly for $ZnAl_{075}Fe_{1.25}O_4$ using EDA as ligand, lattice strain is noted to be about 0.00815, 0.0465, 0.0388 and 0.0682 respectively with increase in annealing temperatures 150°C, 350°C, 650°C and 950°C.

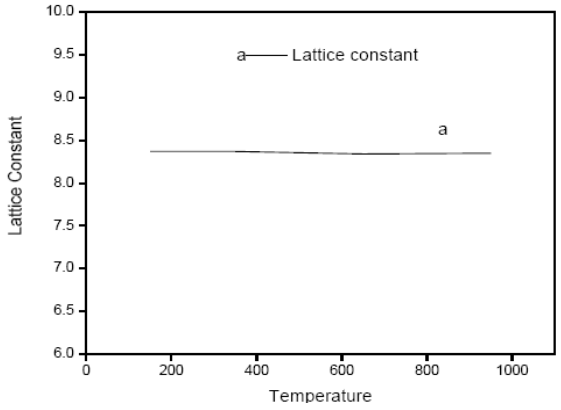

Figure 13. Variation of Lattice constant for $ZnAl_{05}Fe_{1.5}O_4$ using EDA as ligand with temperature

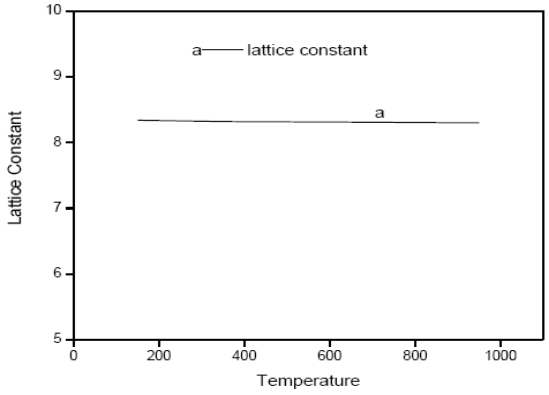

Figure 14. Variation of Lattice Constant for $ZnAl_{075}Fe_{1.25}O_4$ using EDA as ligand with temperature

Figure 13 & 14 reveals the variation of lattice constant for Al substituted Zinc ferrite (x=0.5, 0.75) using EDA as ligand with similar temperature variation. For both case lattice constant variation is similar trend having constant value throughout irrespective of Al^{3+} substitution (x=0.5 mole fraction, x=0.75 mole fraction) noted to be around 8.40Å. Actual values of lattice strain calculated from βCosθ/λ and Sinθ/λ, strain is calculated while d spacing is noted from JCPDS along with planes of direction. Using the formula from Braggs Law lattice constant is calculated as $d = a\sqrt{(h^2 + K^2 + l^2)}$ where a is the lattice constant of the required crystal structure, h, k, l are the planes of orientation. From calculations, it is noted that there is minor reduction in lattice constant as Al^{3+} get substituted for Fe^{3+} in the matrix of Zinc ferrite. Cationic radius of Al^{3+} =0.53Å while that of Fe^{3+} = 0.64Å which indicates clearly that substitution will leads to minor reduction in lattice constant. The exact values of lattice constant for x=0.5 mole Al^{3+} substitution with fixed EDA as ligand are noted as 8.37Å, 8.34Å and 8.35Å for ascending order of four different annealing temperatures. Similarly, for x=0.75 mole Al^{3+} substitution lattice parameters are noted as 8.34Å, 8.32Å, 8.31Å and 8.30Å for ascending order of four different annealing temperatures.

4. Conclusions

Al substituted Zinc ferrite having x=0.5, .75 molar ratio of stoichometry $ZnAl_xFe_{2-x}O_4$ is synthesized using Ethylene diamine as ligand by complexation reaction at about 180°C followed by annealing 150°C, 350°C, 650°C and 950°C for 2 hours. Thermal analyses by DSC-TGA are carried to determine the complexation reaction while the crystallite size is estimated to be about 5.45 to 16.69nm for all cases by Scherrers formula. From strain calculation, plotting of sinθ/λ and βcosθ/λ indicate coefficient of regression R^2 to be close to unity for most cases. In case of 0.5 molar fraction of Al^{3+} substitution R^2 is close to unity with negligible deviation and such is possible with particle size having monodispersive nature. Similar observation is observed for 0.75 mole Al^{3+} substitution with only one deviation in linearity at lower temperature of annealing. Grain size is noted to be increasing with temperature for both Scherrers and Williamson-Hall calculations for both molar Al^{3+} substitutions. Strain induced at lattice within the matrix is found to be decreasing with increase in temperature for both molar substitutions. Lattice constant is found to be nearly constant for molar ratio variation of 0.5 and 0.75 at Fe site. In reality there is slight decrease in lattice parameter since Al^{3+} radius is smaller than Fe^{3+} at B site.

References

[1] Simab Gul, Muhammad Asif Yousuf, Asima Anwar,

 DOI: https://doi.org/10.30564/omms.v2i2.1863

Muhammad Farooq Warsi, Philips O Agboola, Imran Shakir, Muhammad Shahid. Al Substituted Zinc Spinel Ferrite Nanoparticles: Preparation and Evaluation of Structural, Electrical, Magnetic and Photocatalytic Properties. Ceramics International, 2020. https://doi.org/10.1016/j.ceramint.2020.02.228

[2] J. Hu, X. Liu, X. Kan, S. Feng, C. Liu, W. Wang, K.M.U. Rehman, M. Shazed, S. Zhou, Q. Wu. Characterization of Texture and Magnetic Properties of $Ni_{0.5}Zn_{0.5}Ti_xFe_{2-x}O_4$ Spinel Ferrites. Journal of Magnetism and Magnetic Materials, 2019, 489(1). https://doi.org/10.1016/j.jmmm.2019.165411

[3] Li'an Han, Wanlin Zhai, Bing Bai, Huaze Zhu, Jing Yang, Zhengxin Yan, Tao Zhang. Critical behavior in $Ni_{0.15}Cu_{0.15}$ $Zn_{0.7}Fe_2O_4$ spinel ferrite. Ceramics International, 2019, 45(11): 14322-14326.

[4] Chandan Upadhyay, H.C. Verma. Cation distribution in nanosized Ni-Zn ferrites. Journal of Applied Physics, 2004, 95(10): 5746-5751.

[5] Xiuling Jiao, Dairong Chen, Yong Hu. Hydrothermal synthesis of nanocrystalline $M_xZn_{1-x}Fe_2O_4$ (M=Ni, Mn, Co; x=0.40-0.60) powders. Materials Research Bulletin, 2002, 37(9): 1583-1588.

[6] Viorica Musat Bujoreanu, Eugen Segal. On the dehydration of mixed oxides powders coprecipitated from aqueous solutions. Solid State Sciences, 2001, 3(4): 407-415.

[7] Xiao Jia, Dairong Chen, Xiuling Jiao, Tao He, Hanyu Wang, Wei Jiang. Monodispersed Co, Ni-Ferrite Nanoparticles with Tunable Sizes: Controlled Synthesis, Magnetic Properties, and Surface Modification. The Journal of Physical Chemistry C, 2008, 112(4): 911-917.

[8] Adriana S. Albuquerque, José D. Ardisson, Waldemar A. A. Macedo. Nanosized powders of NiZn ferrite: Synthesis, structure, and magnetism. Journal of Applied Physics, 2002, 87(9): 4352-4357.

[9] Wei-Chih Hsu, S.C. Chen, P.C. Kuo, C.T. Lie, W.S. Tsai. Preparation of NiCuZn ferrite nanoparticles from chemical co-precipitation method and the magnetic properties after sintering. Materials Science and Engineering B, 2004, 111(2-3): 142-149.

[10] Chao Liu, Bingsuo Zou, Adam J. Rondinone, Z. John Zhang. Chemical Control of Superparamagnetic Properties of Magnesium and Cobalt Spinel Ferrite Nanoparticles through Atomic Level Magnetic Couplings. Journal of the American Chemical Society, 2000, 122(26): 6263-6267.

[11] A.I. Borhan, P. Samoila, Vasile Hulea, A.R. Iordan, M.N. Palamaru. Effect of Al^{3+} substituted zinc ferrite on photocatalytic degradation of Orange I azo dye. Journal of Photochemistry and Photobiology A: Chemistry, 2014, 279(1): 17-23.

[12] M. Bodzek, M. Rajca. Photocatalysis in the treatment and disinfection of water. Part I. Theoretical backgrounds. Ecological Chemistry and Engineering S, 2012, 19(4): 489-512.

[13] M. Yazdanbakhsh, I. Khosravi, E.K. Goharshadi, A. Youssefi. Fabrication of nanospinel $ZnCr_2O_4$ using sol-gel method and its application on removal of azo dye from aqueous solution. Journal of Hazardous Materials, 2010, 184(1-3): 684-689.

[14] E. Manova, T. Tsoncheva, D. Paneva, I. Mitov, K. Tenchev, L. Petrov. Mechanochemically synthesized nano-dimensional iron-cobalt spinel oxides as catalysts for methanol decomposition. Applied Catalysis A, 2004, 277(1-2): 119-127.

[15] W. Walerczyk, M. Zawadzki, H. Grabowska. Solvothermal synthesis and catalytic properties of nanocrystalline $ZnFe_{2-x}Al_xO_4$ (x = 0, 1, 2) spinels in aniline methylation. Catalysis Letters, 2012, 142(1): 71-80.

[16] R. Spretz, S. Marchetti, M. Ulla, E. Lombardo. Fe/MgO formulations for the catalytic combustion of methane. Journal of Catalysis, 2000, 194(2): 167-174.

[17] J. S. Jang, S. J. Hong, J. S. Lee, P.H. Borse, OK. S. Jung, T. E. Hong, E. D. Jeong, M. S. Won, H. G. Kim. Synthesis of zinc ferrite and its photocatalytic application under visible light. Journal of the Korean Physical Society, 2009, 54(1): 204-208.

[18] M. Amiri, M. Salavati-Niasari, A. Akbari. Magnetic nanocarriers: Evolution of spinel ferrites for medical applications. Advances in Colloid and Interface Science, 2019, 265: 29-44.

[19] M.A. Malik, M.Y. Wani, M.A. Hashim. Microemulsion method: A novel route to synthesize organic and inorganic nanomaterials: 1st Nano Update. Arabian Journal of Chemistry, 2012, 5(4): 397-417.

[20] R. Rameshbabu, R. Ramesh, K. Samikannu, K. Annamalai, S. Ponnusamy. Synthesis and Study of Structural, Morphological and Magnetic Properties of ZnFe2O4 Nanoparticles. Journal of Superconductivity and Novel Magnetism, 2014, 27: 1499-1502.

[21] R. Arulmurugan, B. Jeyadevan, G. Vaidyanathan, S. Sendhilnathan. Effect of zinc substitution on Co-Zn and Mn-Zn ferrite nanoparticles prepared by co-precipitation Journal of Magnetism and Magnetic Materials, 2005, 288: 470-477.

[22] S.U. Rather, O.M. Lemine. Effect of Al doping in zinc ferrite nanoparticles and their structural and magnetic properties. Journal of Alloys and Compounds, 2020, 812: 152058.

DOI: https://doi.org/10.30564/omms.v2i2.1863

BILINGUAL PUBLISHING CO.
Pioneer of Global Academics Since 1984

Non-Metallic Material Science
https://ojs.bilpublishing.com/index.php/nmms

ARTICLE

Synthesis, Electrical Conductivity, and Dielectric Behaviour of Polyaniline Doped with H_2SO_4; HCl and (HCl + $NaNO_2$) Mixture

J. Mohanty[1*] S.S. Mishra[1] T.R. Das Mohapatra[1] S. R. Mishra[2] T. Badapanda[1]

1. Department of Chemistry, C.V. Raman Global University, Bhubaneswar, Odisha, 752054, India
2. Department of Chemistry, Gandhi Institute for Education and Technology, Baniatangi, Odisha, 752060, India

ARTICLE INFO

Article history
Received: 6 September 2020
Accepted: 30 October 2020
Published Online: 30 November 2020

Keywords:
PANI
H_2SO_4
HCl
$NaNO_2$
Dielectric permitivity
Electrical conductivity

ABSTRACT

Acid doped Polyaniline (PANI) due to their increased electrical conductivity, are considered to be the most promising conducting filler materials. Hence, the present study, reports the synthesis of the PANI followed by acid doping, electrical conductivity and dielectric properties measurements of H_2SO_4; HCl and (Conc. HCl + $NaNO_2$mixture) doped PANI. In order to know the effect of acetone washing on the electrical properties of acid doped PANI samples, the electrical properties of the non-acetone washed acid doped PANI samples are compared with that of their acetone washed counterparts. The PANI salt was prepared by conventional route using aniline hydrochloride and ammonium persulphate as an oxidant. PANI salt was subjected to 0.5M NaOH to form PANI base, which was further doped separately with H_2SO_4; HCl and (Conc. HCl + $NaNO_2$mixture) respectively followed by acetone washing. A comparative electrical conductivity study between the acetone washed and unwashed PANI salt and H_2SO_4, HCl and Conc. HCl + $NaNO_2$ mixture doped PANI were characterized by dielectric and impedance study.

1. Introduction

Numerous electrically conductive polymers like polypyrrole, polythiphene, polyparaphenylene and polyaniline though available, but due to the easy synthesis process, greater environmental stability, low cost, polaniline (PANI) is the most studied conducting polymers finding potential electronic applications such as solar cell, light emitting devices, solid state laser, energy storage devices, sensors etc [1-11]. The properties of PANI are determined by the regular structure of polymer chains. The presence of alternating phenyl and nitrogen containing groups as well as the lone pair on nitrogen atom impart polyconjugation, which provides the transport path for charge carrier (formed during oxidation) mobility [12]. The acid doping of polyaniline generates suitable soluble counter-ions which improves the processibility of such conducting polymers. The acid doping of PANI is capable of polyaniline protonation along with providing suitable functional groups to the polymer backbone, making the polymer chemically stable, electrically conductive along with increasing the solubility factor of the polymer [13-16]. The degree of protonation can affect the dielectric, electrical conductivity, and other properties of PANI. The polymerisation of aniline can effectively takes place in acid medium where aniline is present as anilinium ion.

**Corresponding Author:*
J. Mohanty,
Department of Chemistry, C.V. Raman Global University, Bhubaneswar, Odisha, 752054, India;
Email: jayashreemohanty7@gmail.com

 DOI: https://doi.org/10.30564/omms.v2i2.1899

Again, the methodology adopted for preparation of conducting polymers and chemical modifications make them promising candidates for various potential applications. In case of PANI, the polymer is washed with acetone after synthesis for removal of oligomers and other reactive intermediates [17] whose presence is considered to be undesirable in conducting point of view. However, to get an in depth knowledge regarding electrical and optical properties of such conjugated polymer it is essential to study on the short chain oligomers formed during the course of polymerisation and their effects on the overall electrical and optical characteristics of the polymer [2].

In such kind of disordered polymeric system the charge transfer phenomenon is best explained by Complex Impedance Spectroscopy (CIS). It is reported that the hopping of mobile charge carriers is responsible for the electrical conductivity in such a polymeric charge carrier system [18,19]. The variation of electrical conductivity with respect to frequency and dielectric property provide information regarding electronic transport phenomenon in disordered polymeric materials along with the molecular structure of the materials, because due to disorder structure within the material localized electronic states are resulted [20]. In the current manuscript, we have focused the effect of various acids i.e. H_2SO_4; HCl and mixture of HCl + $NaNO_2$ as well as the role of short chain oligomers on the electrical behaviour of PANI via complex impedance spectroscopy.

2. Experimental

The PANI salt was synthesised through the chemical oxidative polymerisation of aniline hydrochloride using oxidant ammonium persulphate. Aniline hydrochloride solution was prepared by dissolving 2.592gm of aniline hydrochloride in 50 ml distilled water. Ammonium persulfate solution was prepared by dissolving 5.704gm in 50 ml. of distilled water. To the aniline hydrochloride solution oxidant ammonium persulfate solution was added slowly with continuous stirring at room temperature and the reaction mixture was allowed to stand for three hour at room temperature followed by filtration. After filtration one part of the residue was washed with 0.2M HCl followed by distilled water and another part was washed with 0.2M HCl and distilled water followed by acetone. The resulting washed PANI samples were dried in air whole night and then at 60^0C in an oven for one day. The resulting dried polymer salt samples were treated with 0.5M NaOH solution and the resulting samples were dried in the similar manner as described for polymer salt samples to prepare PANI base samples. The resulting dried samples were powdered and treated with 1M H_2SO_4, HCl and mixture of HCl and $NaNO_3$. The electrical properties of the synthesized PANI base samples and acid doped PANI samples were measured through making compacted form of circular discs having diameter 10mm and thickness 1mm using a hydraulic press. For electrical contact the ends of the pellets were coated with silver paints. The frequency dependent dielectric and impedance study was carried out by using a N4L-NumetriQ (model PSM1735) connected to a computer.

3. Results and discussion

3.1 *Frequency Dependent* Dielectric Study

The variation of dielectric constant with frequency for PANI base and acid doped PANI samples with and without acetone washing are shown in Figure 1 (a,b). In all the compositions the dielectric constant decreases with increase in frequency which is due to the space charge polarisation produced because of the free charges at the interface [21]. When the frequency is low, the charge carriers get sufficient time to cross the macroscopic distances and accumulates at the interfaces between the sample and the electrodes within half a cycle of the applied AC field, consequently results a high dielectric permittivity [22]. At higher frequencies the plot becomes asymptotic, as expected in case of disordered conducting polymer like PANI, and such trend is occurred due to hopping of electrons between isolated polarons and bipolarons [23]. It is observed from the figure that the acid doping enhances the dielectric constant in the PANI base. In presence of acid the charge carriers are stabilised by the counter ions of the acid which increases the dielectric constant. Again, it can be observed that acetone washing has a great impact on the modification of dielectric behaviour of the doped samples. The acetone washed samples are showing higher dielectric constant in all doped samples. It is also found that for without acetone washed samples maximum dielectric constant was observed for 1MH_2SO_4 doped sample where as for acetone washed composition 1M HCl doped sample is showing highest dielectric constant.

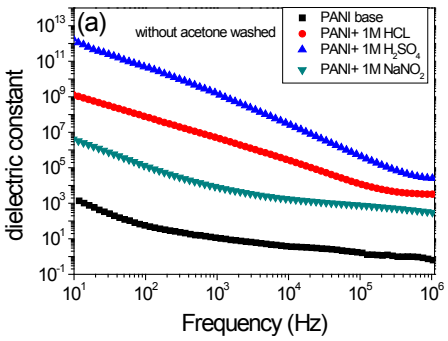

Figure 1 (a). Frequency dependent dielectric constant of without acetone washed acid doped PANI

DOI: https://doi.org/10.30564/omms.v2i2.1899

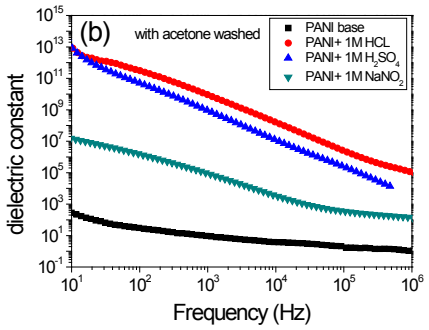

Figure 1 (b). Frequency dependent dielectric constant of acetone washed acid doped PANI

3.2 *AC Conductivity Study*

The frequency dependent AC conductivity of all the non acetone and acetone washed samples respectively are shown in Figure 2(a,b). Using a relation $\sigma ac = \omega\varepsilon\varepsilon_0 \tan\delta$ the AC conductivity is calculated. It has been found that the ac conductivity $\sigma(\omega)$ obeys the Jonscher's power law ($\sigma(\omega) = \sigma_{dc} + A\omega^n$) [24] where n is the frequency exponent in the range of $0 = n = 1$. The factors A and n are temperature dependent parameters suggesting that the electrical conduction is a thermally activated process. Temperature and frequency dependent hopping frequency (ω_p) of the polarons is the frequency at which change in slope takes place and corresponds to short-range hopping of charge carriers through trap sites separated by energy barriers of varied heights. Moreover, non-adiabatic hopping of charge carriers between impurity sites is responsible for the dispersion in conductivity at low frequency. For disordered systems like PANI, movement of electrical charges takes place when it is subjected to an alternating electric field and total conductivity is due to the different types of conduction mechanisms [25]. Such polymers consist of conducting clusters of varying length with random orientation in the absence of the electric field. When the clusters are long enough they can create a percolation path and the charges are free enough to move, hence shows electrical conductivity.

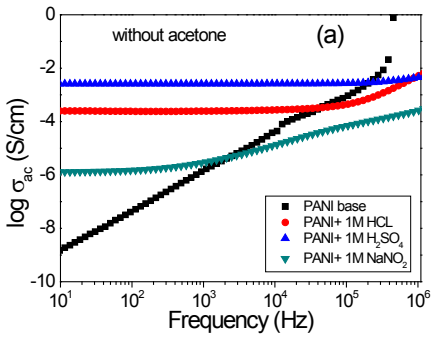

Figure 2 (a). Frequency dependent ac conductivity of without acetone washed acid doped PANI

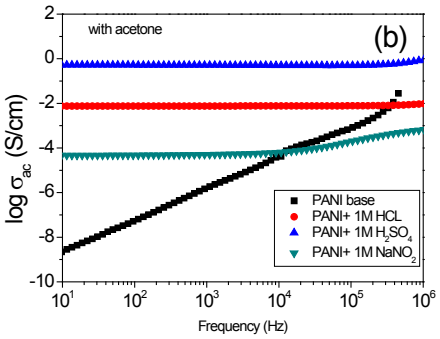

Figure 2 (b). Frequency dependent ac conductivity of with acetone washed acid doped PANI

From Figure 2, it can be observed that for both acetone washed and without acetone washed the doped samples have higher conductivity then that of PANI base. Again, in all doped samples the AC conductivity increases with acetone washing. Another important phenomenon observed with acetone doping is that the hopping frequency move towards the higher frequency side showing that various transport mechanisms are involved in conductivity process. The figure also reveals that with acetone washing there is hardly any decrement of conductivity with frequency in the doped samples which makes the sample more suitable for industrial application then that of the counterpart. Among all the samples, H_2SO_4 doped sample shows highest conductivity for both acetone washed and without acetone washed.

4. Conclusion

Acetone washing has significant effect on the dielectric permittivity of the samples. Among the acid doped samples without acetone washed 1M H_2SO_4 and acetone washed 1M HCl doped PANI samples are considered to be potential dielectric materials. In terms of the electrical conductivity, there is no significant decrement of conductivity with increase in frequency showing their prospects in industrial applications.

References

[1] Chutia P, Kumar A. Physica, 2014, B436: 200.
[2] Salaneck W R, Friend R H, Bredas J L. Physics Reports, 1999, 319: 231.
[3] Ameen S , Ali V , Zulfequar M, Haq M. M, Husain M. Current Appl. Phys, 2007, 7: 215.
[4] Basavaraja C, Kim J K, Thinh P X, Huh D S. Polymer Composites, 2012, 33: 1541.
[5] Cabezas A L, Feng Y, Zheng L R, Zhang Z B. Carbon, 2013, 59: 270.
[6] Hu W, Chen S, Yang Z, Liu L, Wang H. J. Phys.

 DOI: https://doi.org/10.30564/omms.v2i2.1899

Chem. 2011, B115: 8453.
[7] John H,Thomas R M, Jacob J, Mathew K T, Joseph R. Poly. Comp., 2007, 28: 588.
[8] McCall R P, Scherr E M, MacDiarmid A G amd Epstein A J. Physical Review, 1994, 50: 5094.
[9] Upadhyay P K, Ahmad A. Chin. J. Poly. Sci, 2010, 28: 191.
[10] Xue Y, Quesnel D J. RSC Adv., 2016, 6: 7504.
[11] Yoo JE, Cross JL, Bucholz TL, Lee KS, Espe MP, Loo YL. J. of Mater.Chem., 2007, 17: 1268.
[12] Howard R. Synthetic Metals, 1989, 30: 257-263.
[13] Jia QM, Shan SY, Jiang LH, Wang Y.M. Adv. Mater. Res., 2011, 160-162: 1405.
[14] Saravanan S, Joseph C M, Anantharaman MR, Venkatachalam S and Prabhakaran PV. J. Phys. Chem. Solids, 2006, 67: 1496
[15] Chang Q, Li J, Gu D, Yin P, Jiang H and Shen L. J. Macromolecular Science, Part B: Physics, 2015, 54: 381-92
[16] Yoo J.E, Cross JL, Bucholz TL, Lee KS, Espe MP, Loo YL. J. Materials Chemistry, 2007, 17: 1268
[17] Stejskal J, Gilbert R.G., Polyaniline. Preparation of a conducting polymer, Pure Appl Chem, 2002, 74(5): 857-867.
[18] Epstein AJ, MacDiarmid AG. Macromol. Chem. Macromol. Symp., 1991, 51: 11.
[19] Heeger AJ. Faraday Discuss. ChemSoc, 1989, 88: 203-211
[20] Jain H. Experimental Techniques of Glass Science, The American Ceramic Society, Ohio, 1993.
[21] Limelette P, Schmaltz B, Brault D, Gouineau H, Autret-Lambert C, Roger SandGrimal V, Tran VF. J. Applied Physics, 2014, 115: 033712.
[22] McCall RP, Scherr EM, MacDiarmid AG and Epstein AJ. Physical Review B, 1994, 50: 5094.
[23] Epstein AJ, MacDiarmid AG. Macromol. Chem. Macromol. Symp., 1991, 51: 11.
[24] Mrlik M, Moucka R, Iicinova M, Stejskel J. Synthetic metals, 2014, 192: 37-42.
[25] Limelette P, Schmaltz B, Brault D, Gouineau H, Autret-Lambert C, Roger SandGrimal V, Tran VF. J. Applied Physics, 2014, 115: 033712.

DOI: https://doi.org/10.30564/omms.v2i2.1899

BILINGUAL PUBLISHING CO.
Pioneer of Global Academics Since 1984

Non-Metallic Material Science
https://ojs.bilpublishing.com/index.php/nmms

REVIEW

Opinion: Chemical --Mesoscopics..for the Mesoparticles Reactivity Explanation

V.I. Kodolov[1,2*] V.V. Kodolova-Chukhontseva[3]

1. Basic Research - High Educational Centre of Chemical Physics and Mesoscopics, Udmurt Federal Research Centre, UD, RAS, Izhevsk, Russia
2. M.T. Kalashnikov Izhevsk State Technical University, Izhevsk, Russia
3. Institute Macromolecular Compounds, RAS, StPetersburg, Russia

ARTICLE INFO

Article history
Received: 6 September 2020
Accepted: 30 October 2020
Published Online: 30 November 2020

Keywords:
Kolmogorov-Avrami equation
Relative energetic and volume characteristics
Semi empiric Taft constants
Reaction series notion in chemical processes

ABSTRACT

The estimation of chemical particles reactivity and the determination of chemical reactions direction are the actual theme in new scientific trend - Chemical Mesoscopics. Paper includes the proposal about the using the theory of free energy linear dependence from physical organic chemistry and their applications for prognosis of reactions flowing. The semi-empiric constants is given according to mesoscopic physics definitions as well as the transformed Kolmogorov-Avrami equation is discussed. It is the development of Chemical Mesoscopics for organic reactivity estimation including nanostructures reactivity.

1. Introduction

Chemical Mesoscopics is based on the notions about self organization and self similarity [1].

According to the fractal theory [1] any system can be presented as aggregate of elements similar to whole system. These elements have own energetic and geometric (volume) parameters owing to which they are found within the system. The change of these parameters because of the action of external factors leads to disturbance of system balance. At this case the system is destructed or transformed. The estimation of these changes is possible with the using of the relative parameters in which the energetic and volume values are compared with the definite standard values for the correspondent elements (fragments) in the definite reaction series. This approach to reactivity consideration is near to Taft and Pal'm theoretical works [2]. For the relative energetic parameters the following formula $(\varepsilon-\varepsilon_0)/\varepsilon_0$ is proposed [3], where ε_0 corresponds to the surface energy for standard chemical fragment. In turn, analogous relative parameters are proposed [4] for the volume characteristics $(V-V_0)/V_0$.

**Corresponding Author:*
V.I. Kodolov,
Basic Research - High Educational Centre of Chemical Physics and Mesoscopics, Udmurt Federal Research Centre, UD, RAS, Izhevsk, Russia;
M.T. Kalashnikov Izhevsk State Technical University, Izhevsk, Russia;
Email: vkodol.av@mail.ru

 DOI: https://doi.org/10.30564/omms.v2i2.2440

2. Discussion

The development of Chemical Mesoscopics in this direction is connected with the research of the size and energetic characteristics of chemical particles. The size of mesoparticles is denoted as approximately 10 nm, and the motion freedom of nanostructures (mesoparticles) is limited by the vibration with high frequency and electron transport across them. The peculiarities of mesoparticles consist in the radiation of energy quants of negative or positive charges. This radiation is the main reason of the stimulation of chemical processes. At the imposition of the negative charge quants the interference takes place and the chemical bonds are formed. In turn the imposition of the negative and positive quants together the phenomenon of annihilation is created. At this case the direct electromagnetic field is appeared that leads to the stimulation of negative charge quants moving and the growth of chemical bonds formation. The phenomena of interference and annihilation are reasons of start for self organization process with reservation conformation order, which determine the finished product structure. For the process explanation the equation of Kolmogorov-Avrami [1] can be used -

$$W = 1 - \exp(-k\tau^n), \quad (1)$$

where W - the part of obtained product (for instance, polymer), k - the process rate constant, τ - the duration of process, n - the fractal dimension (for one measured process n = 1).

For the comparative estimation of reagents (or nanostructures) in one reaction series it's possible the application of the theory of free energy linear dependences. In this case the reactions are considered with using one of reagent as the standard compound for which W is fixed W_0. The estimation of reactivity can be proposed on the difference $W-W_0$, where W is calculated on formula 2, and W_0 is defined on analogous formula with changes $k_0\tau_0^n$. It's noted, the fractal dimension n do not change because the comparison is carried out for one type of reactions. The following equation for difference $W - W_0$ can be written -

$$W - W_0 = \exp(-k_0\tau_0) - \exp(-k\tau^n) \quad (2)$$

and after eq. 2 transformation -

$$W_0 = k/k_0\,(\tau/\tau_0)^n - 1 \quad (3)$$

If $\lg k/k_0$ is defined as -

$$\lg k/k_0 = -2{,}3\,RT\,\{[(\varepsilon_0 - \varepsilon)/\varepsilon_0]a + [(V_0 - V)/V_0]b\} \quad (4)$$

and then this expression after transformation stand in the eq. 3, than the equation 5 is received -

$$\lg (W - W_0) = (\tau/\tau_0)^n \exp\{[(\varepsilon_0 - \varepsilon)/\varepsilon_0]a + [(V_0 - V)/V_0]b\} \quad (5)$$

where values a and b - parameters, which correct the influence polar and steric (spaced) effects on reactivity in polymerization, the relation $(\varepsilon_0 - \varepsilon)/\varepsilon_0$ [3,4] correspondents to Taft constant σ (polarity constant), and the relation $(V_0 - V)/V_0$ - Taft constant E_s (steric or spaced constant) [3].

3. Conclusion

The application of above notions for the Chemical Mesoscopics development is very perspective because stimulates the mathematic apparatus creation for the chemical processes flowing direction prediction.

References

[1] V.I. Kodolov, V.V. Kodolova-Chukhotzeva. Fundamentals of Chemical Physics. Izhevsk: M.T. Kalashnikov IzhSTU, 2019: 218.

[2] V.A. Pal'm. The introduction in theoretical organic chemistry. M.: Publ. "High School", 1974: 446.

[3] V.I. Kodolov. Possibilities of modeling in organic chemistry. Organic Reactivity, 1965, 2(4-6): 11-17.

[4] V.I. Kodolov, S.S. Spasskiy. Parameters in Alfrey-Price and Taft equations. Vysokomol. Soed., 1976, 18(9): 1986-1992.

DOI: https://doi.org/10.30564/omms.v2i2.2440

BILINGUAL PUBLISHING CO.
Pioneer of Global Academics Since 1984

Non-Metallic Material Science
https://ojs.bilpublishing.com/index.php/nmms

ARTICLE

A Potential Approach to Enhance the Seebeck Coefficient of UHMWPE by Using the Graphene Oxide

Aqsa Irfan[1] Malik Naqash Mehmood[2] Malik Sajjad Mehmood[1*] Arif Aziz[3]
Mansoor Ahmad Baluch[1] Muhammad Rizwan[2] Tariq Yasin[4]

1. Department of Basic Science, University of Engineering and Technology, Taxila, 47050, Pakistan
2. Department of Physics, Air University, 444000, Islamabad, Pakistan
3. Harbin Engineering University, Harbin, Heilingjiang, 150001, China
4. Department of Chemistry, Pakistan Institute of Engineering and Applied Sciences, 45650, Islamabad, Pakistan

ARTICLE INFO

Article history
Received: 6 September 2020
Accepted: 30 October 2020
Published Online: 30 November 2020

Keywords:
UHMWPE
Graphene oxide
Electrical conductivity
Thermal conductivity
Seebeck coefficient
Figure of merit

ABSTRACT

Thermoelectric materials have been a competent source for the production of energy in the present decade. The most important and potential parameter required for the material to have better thermoelectric characteristics is the Seebeck coefficient. In this work, ultra high molecular weight polyethylene (UHMWPE) and graphene oxide (GO) nanocomposites were prepared by mechanical mixing by containing 10000ppm, 50000ppm, 70000ppm, 100000ppm, 150000ppm, and 200000ppm loadings of graphene oxide. Due to the intrinsic insulating nature of UHMWPE, the value of Seebeck for pristine UHMWPE and its nanocomposites with 10000ppm & 50000ppm of GO concentration was too low to be detected. However, the Seebeck coefficient for composites with 70000ppm, 100000ppm, 150000ppm, and 200000ppm loadings of GO was found to be 180, 206, 230, and 235 μV/K, respectively. These higher values of Seebeck coefficients were attributed to the superior thermal insulating nature of UHMWPE and the conductive network induced by the GO within the UHMWPE insulating matrix. Although, the values of the figure of merit and power factor were negligibly small due to the lower concentration of charge carriers in UHMWPE/GO nanocomposites but still reported, results are extremely hopeful for considering the composite as the potential candidate for thermoelectric applications.

1. Introduction

Due to the excessive use of natural resources for power generation, i.e. of 4.1×10^{20} J, thermoelectric materials are coming to the limelight for the advantage of conversion of heat energy into electrical energy and vice versa. It is based on the thermoelectric effect with Seebeck effect (conversion of heat energy into electrical energy), Peltier effect (conversion of electrical energy to heat energy), and Thomson effect (conductor heating/cooling). These physical phenomenons can be used for the conversion of heat from home, industries, and many other sources into

**Corresponding Author:*
Malik Sajjad Mehmood,
Department of Basic Science, University of Engineering and Technology, Taxila, 47050, Pakistan;
Email: msajjad.82@gmail.com

 DOI: https://doi.org/10.30564/omms.v2i2.2601

useful electricity by means of thermoelectric materials. Thermoelectric generators are basically solid state devices, ideal for small scale power generation with salient features of fixed parts, zero noise, and highly reliable [1]. The efficiency of thermoelectric material is a function of the figure of merit $ZT = (\sigma S^2/K)T$, where σ is the electrical conductivity in units of Siemens per meter, S is the Seebeck coefficient in units of volts per degree, K is the thermal conductivity in units of Watts per degree per meter and the units of Z are the inverse of temperature, so that ZT is dimensionless, where T is the absolute temperature in units of Kelvin. The more efficient thermoelectric materials have high electrical conductivity, low thermal conductivity, and high Seebeck coefficient.

The most commonly used thermoelectric materials were Bismuth telluride (Bi_2Te_3), Lead telluride (PbTe), Tin Selenide (SnSe), Silicon-Germanium alloys, however; the problem such as the involvement of harmful materials and difficulties in processing were the major constraints. It is therefore, researchers are working to replace the aforementioned materials with conducting polymers [2]. Among the various conducting polymers, polyaniline (PANi) and poly (3,4-ethylenedioxythiophene)-poly(styrenesulfonate) (PEDOT:PSS), Poly(3-hexylthiophene) (P3HT), and their derivatives are promising candidates of thermoelectric (TE) materials. Majority of polymers, other than conductive ones, have low electrical conductivity, which is the major limitation for using polymers as TE materials with reasonable confidence. To overcome this limitation, conductive nanofillers are introduced in polymers to retune their electrical and thermal conductive properties. Among these fillers, graphene based nanofillers i.e. graphene, reduced graphene oxide, graphene oxide (GO) nanoparticles, and graphene nanoplatelets are suitable conductive filler in insulating polymers for required thermoelectric applications because of their excellent electronic, electrical, optical, thermal, and mechanical properties with large surface area [3].

For the first time, thermoelectric properties of PANI/GNs were reported by Du et al., [4] using the ratios of 4:1, 3:1, 2:1, and 1:1 of polyaniline and graphene nanosheets, respectively. The values of figure of merit, i.e., ZT for films and pallets were found to change from 0.05 to 1.47 and from 0.64 to 5.60 $\mu Wm^{-1}K^{-2}$, respectively. Xiang et al., [5] prepared graphene nanoplatelets (GNP) based polyaniline composites and reported the values of Seebeck coefficient and electric conductivity σ 33μV/K and 59 S/cm, respectively for the sample containing the 40 wt% of PANI. The major novelty of this work was the in-situ polymerization of aniline monomers for composite preparation. Yoo et al., [6] were the first to prepare the composites of PEDOT: PSS with 3 wt % of graphene. The following results were obtained in this study:

(1) The value of electrical conductivity for PEDOT:PSS/graphene composites was 637 Scm^{-1} in this study.

(2) The values of electrical conductivity were found 41% higher for the composites compared to pure PEDOT:PSS film.

(3) The highest thermoelectric power factor of 45.7 $\mu W \cdot m^{-1} \cdot K^{-2}$ was obtained, which is 93% higher than that of the primal PEDOT:PSS film.

Using graphene doping and hydrazine treatment Xiong et al., [7] formulate PEDOT:PSS nanocomposite with the following strange behaviors:

(1) Decreasing behavior of the electrical conductivity was observed with the increase of graphene contents (For 3 wt% graphene decrease in electrical conductivity was from 1298 to 783 S cm^{-1})

(2) A significant increase in thermoelectric power factor was observed, i.e., 53.3 $\mu W.m^{-1}K^{-2}$, which was two times higher than pure PEDOT:PSS

More recently Gao et al., [8] prepared acrylonitrile-butadiene-styrene copolymer/reduced graphene ABS/rGO nanocomposites by latex method. Although, electrical conductivity was noted as high as 0.09 S/m but an increase in thermal conductivity was also found with increasing the contents of graphene was increased in ABS.

This study aims to investigate the feasibility of using a unique, gold standard high strength industrial polymer i.e. Ultra High Molecular Weight Polyethylene (UHMWPE) as thermoelectric material. UHMWPE has been the substitute of many organic materials having a long chains of monomers of ethylene (molecular mass ranges between 3.5 to 7.5 million amu), with the properties of having no odor, no taste, nontoxicity, and abrasion resistant. Due to UHMWPE's high molecular weight, it will not modulus, diffuse, or stream out as a fluid, and can be processed with powder metal technology. The properties of UHMWPE that motivates for analyzing it for the subject matter of interest are its ability to withstand in severe environment, the highest capability of heat insulation/absorption among the family, dissipation of energies from various physical processes like stress, pressure, etc., possibility for inducing the conducting networks within UHMWPE matrix either by incorporating the conductive fillers or by increasing the C=C conjugations and most importantly tuning its electrical conductivity while inducing the free radicals in UHMWPE matrix [9-11].

DOI: https://doi.org/10.30564/omms.v2i2.2601

2. Experimental

2.1 Materials

UHMWPE resin powder, H_2SO_4, H_3PO_4, $KMnO_4$, commercial Graphite, HCl, and water were used for the preparation of UHMWPE/GO nanocomposites.

2.2 Preparation of UHMWPE/GO Composite Pellets

Graphene oxide (GO) was synthesized by a modified Hummer's process in which 1 g of commercial graphite, 8 ml of HCl, and 25 ml of H_2O were stirred under room temperature for 30 min and allowed to settle down. After decantation, washing of the precipitate was performed with distilled water continuously until it achieved pH 7. The precipitates were then left over for 12-16 h at room temperature to obtain expanded graphite having a silverish black color. After obtaining the expanded graphite, a mixture of 1 g of expanded graphite, 40 ml of H_2SO_4, and 3.9 ml of H_3PO_4 was placed in an ice bath (0-5 °C) and continuously stirred for 30 min. After this mixture was slowly removed from the ice bath and 1.8 g of $KMnO_4$ was added, the admixture was then continuously stirred for 30 min at a temperature below 5 °C. Subsequently, 10-15 ml of H_2O was added to the mixture at room temperature and placed on the magnetic stirrer for 15-20 min stirring again, which turned the color of the mixture to reddish brown. This reddish brown mixture was then sealed and boiled to 100 °C and stirred for the next 2 h which changes its color from reddish-brown to bright yellow. The bright yellow solution was diluted by adding 15 ml of H_2O and 4-5 ml of H_2O_2, stirred at room temperature for 30 min, and the solution is allowed to settle down overnight after that decantation of the upper clear half was performed. The subsequent blend were washed over and over by centrifugation with 10% HCl and deionized water for a few times until it turned to gel-like substance having pH=7. After the process of filtering, drying, centrifuging at 80 °C for 6 h, and sonication for 5 hours in H_2O_2, the graphene oxide (GO) was obtained as a black powder.

To get the UHMWPE/GO pellets, the mixture of UHMWPE and graphene oxide nanoparticles were prepared having 1wt.%, 5 wt.%, 7 wt.%, 10 wt.%, 15 wt.%, and 20 wt.% of graphene oxide. To obtain the homogenous mixture, the mechanical mixture available at Pakistan Institute of Engineering and Applied Sciences PIEAS was used, and each mixture was mixed mechanically for 120 minutes. Afterward, each mixture was pressed in the shape of pellets having the thickness=4mm, diameter =13mm. The pressing was done with the help of a manual laboratory hydraulic press available at PIEAS. The pressure during the fabrication of pellets was slowly varied from 50 to 200 MPa. The pressure rose gradually from lower to a higher value. At maximum values, a holding time of 20 mints were given to have compact pellets. It is worth mentioning here that the whole compaction process was carried out at room temperature. Subsequent to compaction, the pressure was removed and pellets were placed on the shelf for the next 24 hours to ensure their quality of each formulation compaction.

2.3 Characterization of UHMWPE/GO Composite Pellets by X-ray Diffraction

X-ray diffractometer (Model X' TRA48, Thermo ARL) was used for X-ray diffraction analysis. The operational voltage of the instrument was 45 kV and a current of 40 mA was applied. Using the famous Bragg's equation, the inter layer spacing d_{hkl} was calculated

$$d_{hkl} = \frac{n\lambda}{sin\theta}$$

Where n, λ and θ are the diffraction level, wavelength, and the Bragg's angle, respectively while hkl are the lattice planes. The wavelength of the X-ray was 1.541 Å. The data was collected in the reflection mode from 5° to 60° at a scanning rate of 10° min^{-1}. The average crystallite size (D) normal to the lattice plane was acquired by utilizing Scherer's formula given as:

$$D = \frac{K\lambda}{\beta cos\theta}$$

Where β is the full width at half maxima (FWHM) in radians *K* is crystal factor and is equal to 0.89. The lattice parameter was calculated using the following equation

$$a = \frac{\lambda}{2sin\theta}\sqrt{h^2 + k^2 + l^2}$$

The % crystallinity of nanocomposites was calculated while using the following equation

$$X_c(\%) = \frac{Total\ area - Peak\ amorphous\ area}{Total\ area} \times 100$$

2.4 Characterization of Physical Properties

Electrical conductivity of UHMWPE/GO composites is measured by four-point probe method. The voltage data is obtained from the inner two ends while the current data is obtained from the outer 2 ends. It is worked by contacting 4 equally spaced, co-linear copper electrodes coated on the glass substrate with the material. The electrical conductivity of composites along with cross-sectional area A and length l is determined by:

 DOI: https://doi.org/10.30564/omms.v2i2.2601

$$\sigma = \frac{I}{V} \times \frac{l}{A} = \frac{I}{V} \times \frac{l}{f.w}$$

Where

I = current flow through the outer electrode

V = voltage measured at the inner electrodes

f = pellet thickness

w = pellet width

Thermal conductivity is the ability of the material to carry out or transfer heat that is influenced by temperature, chemical composition, and microstructure. It is an experimental parameter rich in microscopic information. Sample's thermal conductivity is measured by the Lee Disk method by steady state technique. Steady state is defined by no variation of current for a specific time, i.e, no heat enters or leaves the system.

To obtain accurate readings, UHMWPE/GO is placed on one of the brass discs that should be wrapped in thermal insulator cotton. One disc is heated and the other is not. Loss of heat by conduction and convection to the environment (air) can skew the results obtain, thus using an insulating material where appropriate is important to obtain proper results using Lee's Disc method. At equilibrium, the heat transfer is equal to the electric power.

$$Heat\ flow\ rate\ (Q) = \frac{[\kappa \times A \times (T_1 - T_2)]}{d}$$

Where

κ = Thermal Conductivity (W/mK)

A = Pellet area (m^2)

T_1 and T_2 = Temperature (K)

d = length with which the heat travel (m)

Q = Rate of heat transfer (W)

For Seebeck coefficient measurement, the UHMWPE/GO composites are provided with a temperature gradient. One edge of the pellet is activated at higher temperature while the second one is maintained to be at lower temperature by means of two gradient heaters to achieve the difference. The voltage is calculated by Textronix DM 5120, these voltages are Seebeck voltage which is the potential difference calculated by the Sample pellet differential thermocouple (DTC). The potential difference, calculated by Keithley 195A DMM, is basically due to the temperature difference across the plates. After measurement, the data is plotted on the software origin, and a plot of ΔV vs ΔT is obtained for the estimation of Seebeck coefficient.

3. Results and Discussion

3.1 Structural Analysis of UHMWPE/GO Composite Pellets

To precede the investigation of the impact of graphene oxide inclusions in the crystalline structure of UHMWPE, X-ray diffraction analysis has been conducted. Figure 1(a) expresses the graphs of virgin UHMWPE, and 1%, 15%, and 20% of GO composites embedded in UHMWPE substrate. Two sharp narrow peaks at the angle of 2θ = 21.5° (110) and 2θ= 24°(200) of each image shows the orthorhombic crystallographic planes of UHMWPE in reference to work reported in the literature [10,12,13]. Figure 1(b) shows the phase analysis of raw UHMWPE with intense sharper peaks with a significant amount of amorphous area. It is evident from results that the addition of graphene oxide results in a decrease in the crystalline peaks of both reflection planes for all samples. The reduction in the intensity peak of the 1% sample is higher than that of other percentages. Further increase in graphene oxide content again caused the recovery of sharpen peaks. Plasticity induced by GO within the matrix of UHMWPE is attributed to the variation in chain breakage that occurs close to the crystalline lamellae.

It is also cleared from the images that it has no characteristic broad peak of graphene oxide at the angle of 25.5°, however, some broadness at 30° (figure 1(b)) predicts the complete dispersion of GO composites in the substrate. Another evidence of complete dispersion of GO was the sudden decrease in intensity of 1% UHMWPE/GO compared to that of virgin UHMWPE. GO cause the loosening and breakage in the links of the mother substrate and lead to less crystalline phase [14]. The parameters for all samples obtained during x-ray analysis are listed in Table 1.

Table 1. Parameters from the X ray diffraction analysis

Sample	Angle 2θ	hkl	d(nm)	a(nm)	FWHM	Crystallite size	Percentage crystallinity(%)
P	21.51	110	0.4127	0.7194	0.6331	0.2228	46.18
	23.91	200	0.3718	0.7437			
PG_1	21.44	110	0.4141	0.7172	0.7685	0.2343	29.82
	23.81	200	0.3718	0.7466			
PG_5	21.45	110	0.4138	0.7167	0.7157	0.1971	39.05
	23.84	200	0.3728	0.7456			
PG_7	21.55	110	0.4119	0.7135	0.7970	0.1770	40.66
	23.92	200	0.3716	0.7432			
PG_{10}	21.50	110	0.4128	0.7151	0.7140	0.1975	41.28
	23.65	200	0.3758	0.7517			
PG_{15}	21.48	110	0.4132	0.7158	0.6385	0.2270	41.72
	23.89	200	0.3717	0.7441			
PG_{20}	21.52	110	0.4125	0.7144	0.6209	0.2272	43.37
	23.91	200	0.3717	0.7434			

DOI: https://doi.org/10.30564/omms.v2i2.2601

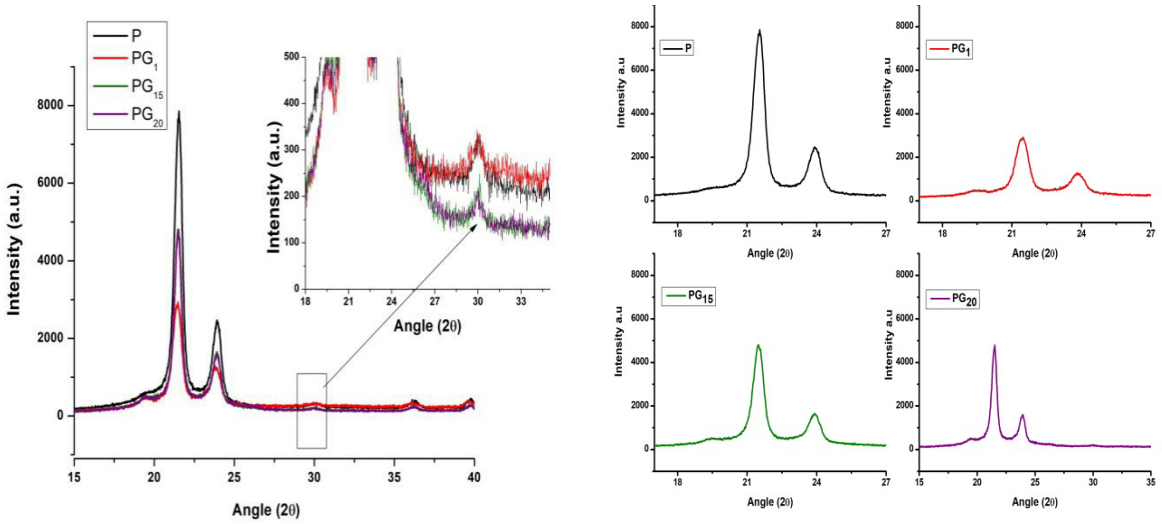

Figure 1. (a) X ray diffraction of the sample of different ratios; (b) Broadness of graphene oxide particles

Note:
P: pure UHMWPE, PG1: 1%GO in UHMWPE, PG15: 15% GO in UHMWPE, PG20: 20% UHMWPE.

3.2 Thermoelectric Properties of UHMWPE/GO Composite Pellets

Figure 2(a) shows the variation of conductivity vs temperature for 7%, 10%, 15%, and 20% content of graphene oxide. There is an irregular variation of current with an increase of temperature for 7%. For the nonconductors, the electrical conductivity is considered as low as less than 10^{-8} S/m and the electrical conductivity range for 7% is between 10^{-9} and 10^{-8} S/m so apparently, we don't consider it as conductor. When GO content reaches to 10%, the conductivity slowly increases with the increase in temperature, this is because GO has greater aspect ratio and its small amount causes the breakage in the links of UHMWPE and forms the conductive path. However, in the case of 15% and 20% content, there is stability in conductivity with an increase in temperature as graphene oxide begins to strengthen the substrate after influencing the linkage breaks. Hence, more GO content causes a decrease in resistivity of our polymer.

The relationship between thermal conductivity, thermal diffusivity, and volumetric heat capacity of UHMWPE-GO composites and the corresponding content of GO in UHMWPE substrate is illustrated in figure 2(b). Thermal

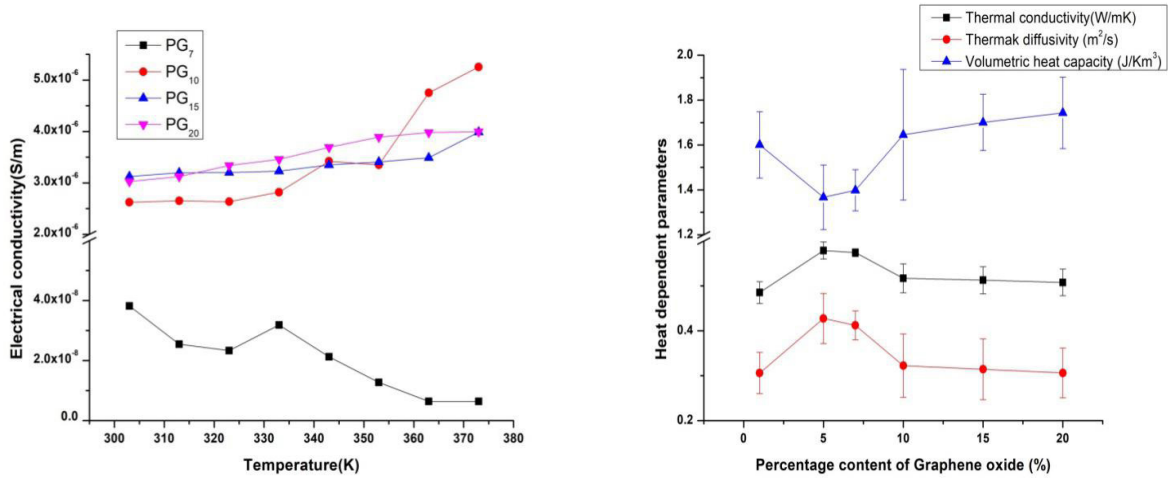

Figure 2. (a) UHMWPE/GO electrical conductivity variation with temperature for 7%, 10%, 15%, and 20% GO content; (b) Variation of thermal conductivity, thermal diffusivity, and volumetric heat capacity with graphene oxide content in UHMWPE

 DOI: https://doi.org/10.30564/omms.v2i2.2601

conductivity increases with the increase of GO content up to 5% and the curve is linear. For 7% content, there is a small abate in thermal conductivity, and further addition of 10% content causes more drop in thermal conductivity approach to 0.51W/mK and for 15% and 20% content very small declination is observed. This trend shows that if we further increase the GO content, thermal results in the decline of thermal conductivity. In essence, phonons are treated as thermal conductivity carriers. The phonons of GO nanoparticles do not counterpart with the phonons of the UHMWPE, which verdict in a large thermal resistance due to the boundaries of graphene oxide, so the property of thermal conductivity of the UHMWPE/GO composites is restrained. The main reason for the deceased conductivity is that the graphene makes the diffusion of heat slower, as a result vibration and rotation of atoms become dislocated. Thermal diffusivity of our composite showed the same behavior as the thermal conductivity but in lower values. While the trend of volumetric heat capacity is completely in contrast to that of thermal conductivity with much larger values.

Since Seebeck coefficient is totally independent of dimension, so sample geometry doesn't concern. It is obvious that there is no electrical conductivity observed for pure, 1% and 5% content. As the Seebeck coefficient depends on electrical conductivity, so there is no variation in the voltage output to temperature difference ratio. It is illustrated by figure 3(a), the Seebeck coefficient of 7%, 10%, 15% and 20% nanocomposite material increase with the increase in the amount of GO in UHMWPE ranges from 180 to 235μV/K at room temperature.

The efficiency of thermoelectric material is expressed by the figure of merit. Figure 3(b) gives the reliance of the figure of merit of UHMWPE/GO nanocomposites with the increased fraction of graphene oxide. The figure of merit shows the rapid growth from 7% to 10% content. Although the Seebeck coefficient of 7% content is quite higher, yet its electrical conductivity is much lower, i.e, in 10^{-8} S/m that causes the lower efficiency of this sample. With the increment of graphene oxide from 10% to 15% and 20%, the figure of merit shows the higher values as their respective electrical conductivities and Seebeck coefficients increase with a little bit of consistency in thermal conductivity. Furthermore, these values of the figure of merit are quite not suitable for common applications, but there may be further ways of improvement.

Parameters upon which the figure of merit depends at 303K are listed in Table 2

Table 2. Summarized values of thermoelectric properties of UHMWPE/GO composites at room temperature

Sample	Electrical conductivity σ (S/m)	Seebeck coefficient S (V/K)	Power factor σS^2 (W/mK^2)	Thermal conductivity κ (W/mK)	Figure of merit ZT
P	0	0	0	0.4852	0
PG_1	0	0	0	0.5789	0
PG_5	0	0	0	0.5741	0
PG_7	3.82166E-08	1.80E-04	1.23822E-15	0.5168	7.25967E-13
PG_{10}	2.62208E-06	2.06E-04	1.11271E-13	0.5142	6.55679E-11
PG_{15}	3.12E-06	2.30E-04	1.65286E-13	0.5129	9.76441E-11
PG_{20}	3.03E-06	2.35E-04	1.67056E-13	0.5078	9.96807E-11

4. Conclusion

Organic thermoelectric materials are coming to the limelight for the advantage of conversion of heat energy into electrical energy and vice versa. They are preferred

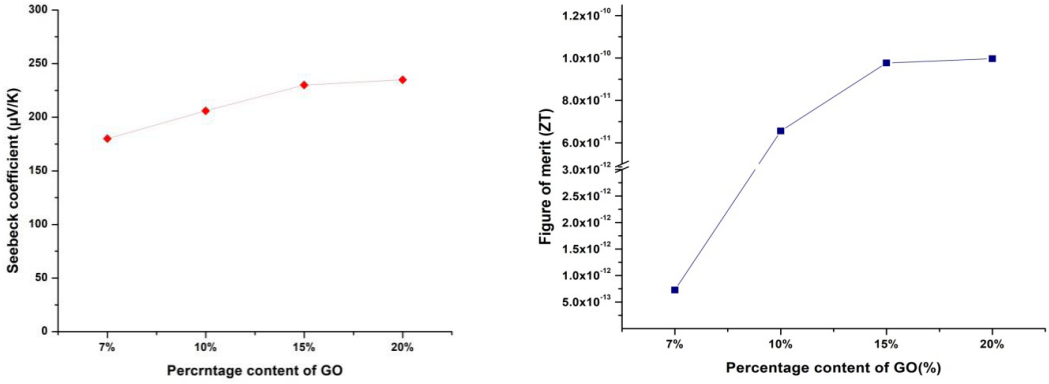

Figure 3. (a) Variation of Seebeck coefficient with respect to increased content of graphene oxide; (b) Reliance of figure of merit on graphene oxide content

DOI: https://doi.org/10.30564/omms.v2i2.2601

over conventional thermoelectric materials due to their higher strength, processability, lower cost, and nontoxic. In the present work, we have done systematic studies on the structural and thermoelectric properties of UHMWPE blended with 1%, 5%, 7%, 10%, 15%, and 20% graphene oxide nanocomposites. Sharp peaks of UHMWPE at 21.5° and 24° with the appearance of graphene at 30° by XRD are obtained. The DC conductivity increases with the increase in the concentration of graphene oxide nanoparticles with the increase in temperature. The thermal conductivity decreases with the increase in graphene oxide content at room temperature. The Seebeck coefficient increases with the increase in graphene oxide concentration. As we measured, the Seebeck coefficient increases with the increase in temperature. Efficiency of UHMWPE/GO nanocomposites is also increased in the scenario of all three parameters.

Although the values of the figure of merit are quite not suitable for common applications yet, there may be further ways of improvement by doping the UHMWPE with higher content of graphene oxide and other highly conductive fillers. All in all, these composites after improved efficiency can be used to supply the energy. It is clearly just a matter of time!

References

[1] G. J. Snyder, E. S. Toberer. Complex thermoelectric materials. In Materials for sustainable energy: a collection of peer-reviewed research and review articles from Nature Publishing Group, ed: World Scientific, 2011: 101-110.

[2] G. Mahan. Introduction to thermoelectrics. APL Materials, 2016, 4: 104806.

[3] Y. Zhu, S. Murali, W. Cai, X. Li, J. W. Suk, J. R. Potts, et al. Graphene and graphene oxide: synthesis, properties, and applications. Advanced materials, 2010, 22: 3906-3924.

[4] Y. Du, S. Z. Shen, W. Yang, R. Donelson, K. Cai, P. S. Casey. Simultaneous increase in conductivity and Seebeck coefficient in a polyaniline/graphene nanosheets thermoelectric nanocomposite. Synthetic Metals, 2012, 161: 2688-2692.

[5] J. Xiang, L. T. Drzal. Templated growth of polyaniline on exfoliated graphene nanoplatelets (GNP) and its thermoelectric properties. Polymer, 2012, 53: 4202-4210.

[6] D. Yoo, J. Kim, S. H. Lee, W. Cho, H. H. Choi, F. S. Kim, et al. Effects of one-and two-dimensional carbon hybridization of PEDOT: PSS on the power factor of polymer thermoelectric energy conversion devices. Journal of Materials Chemistry A, 2015, 3: 6526-6533.

[7] J. Xiong, F. Jiang, H. Shi, J. Xu, C. Liu, W. Zhou, et al. Liquid exfoliated graphene as dopant for improving the thermoelectric power factor of conductive PEDOT: PSS nanofilm with hydrazine treatment. ACS Applied Materials & Interfaces, 2015, 7: 14917-14925.

[8] A. Gao, F. Zhao, F. Wang, G. Zhang, S. Zhao, J. Cui, et al. Highly conductive and light-weight acrylonitrile-butadiene-styrene copolymer/reduced graphene nanocomposites with segregated conductive structure. Composites Part A: Applied Science and Manufacturing, 2019, 122: 1-7.

[9] S. A. Maqbool, M. S. Mehmood, S. S. Mukhtar, M. A. Baluch, S. Khan, T. Yasin, et al. Dielectric relaxation and acconduction in γ-irradiated UHMWPE/MWCNTs nano composites: impedance spectroscopy analysis. Radiation Physics and Chemistry, 2017, 134: 40-46.

[10] M. S. Mehmood. Characterization of gamma sterilized and cross-linked vitamin-E stabilized ultra-high molecular weight polyethylene. Pakistan Institute of Engineering & Applied Sciences, Islamabad., 2013.

[11] M. S. Mehmood, M. S. Jahan, T. Yasin, M. Tariq, M. A. Choudhry, M. Ikram. On the structural analysis of [gamma]-ray induced primary free radicals in UHMWPE and vitamin E stabilized UHMWPE by ESR spectroscopy. Journal of Spectroscopy, 2015, 2015.

[12] M. S. Mehmood, T. Yasin, M. S. Jahan, S. R. Mishra, B. M. Walters, M. Ahmad, et al. Assessment of residual radicals in γ-sterilized shelf-aged UHMWPE stabilized with α-tocopherol. Polymer degradation and stability, 2013, 98: 1256-1263.

[13] M. S. Mehmood, B. M. Walters, T. Yasin, M. Ahmad, M. S. Jahan, S. R. Mishra, et al. Correlation of residual radical's with three phase morphology of UHMWPE: Analysis for the dependence on heat involved during vitamin E diffusion. European polymer journal, 2014, 53: 13-21.

[14] H. Bahrami, A. Ramazani SA, A. Kheradmand, M. Shafiee, H. Baniasadi. Investigation of thermomechanical properties of UHMWPE/graphene oxide nanocomposites prepared by in situ Ziegler–Natta polymerization. Advances in Polymer Technology, 2015, 34.

 DOI: https://doi.org/10.30564/omms.v2i2.2601

Author Guidelines

This document provides some guidelines to authors for submission in order to work towards a seamless submission process. While complete adherence to the following guidelines is not enforced, authors should note that following through with the guidelines will be helpful in expediting the copyediting and proofreading processes, and allow for improved readability during the review process.

Ⅰ. Format

- Program: Microsoft Word (preferred)
- Font: Times New Roman
- Size: 12
- Style: Normal
- Paragraph: Justified
- Required Documents

Ⅱ. Cover Letter

All articles should include a cover letter as a separate document.

The cover letter should include:

- Names and affiliation of author(s)

The corresponding author should be identified.

Eg. Department, University, Province/City/State, Postal Code, Country

- A brief description of the novelty and importance of the findings detailed in the paper

Declaration

v Conflict of Interest

Examples of conflicts of interest include (but are not limited to):

- Research grants
- Honoria
- Employment or consultation
- Project sponsors
- Author’s position on advisory boards or board of directors/management relationships
- Multiple affiliation
- Other financial relationships/support
- Informed Consent

This section confirms that written consent was obtained from all participants prior to the study.

- Ethical Approval

Eg. The paper received the ethical approval of XXX Ethics Committee.

- Trial Registration

Eg. Name of Trial Registry: Trial Registration Number

- Contributorship

The role(s) that each author undertook should be reflected in this section. This section affirms that each credited author has had a significant contribution to the article.

1. Main Manuscript
2. Reference List
3. Supplementary Data/Information

Supplementary figures, small tables, text etc.

As supplementary data/information is not copyedited/proofread, kindly ensure that the section is free from errors, and is presented clearly.

Ⅲ. Abstract

A general introduction to the research topic of the paper should be provided, along with a brief summary of its main results and implications. Kindly ensure the abstract is self-contained and remains readable to a wider audience. The abstract should also be kept to a maximum of 200 words.

Authors should also include 5-8 keywords after the abstract, separated by a semi-colon, avoiding the words already used in the title of the article.

Abstract and keywords should be reflected as font size 14.

Ⅳ. Title

The title should not exceed 50 words. Authors are encouraged to keep their titles succinct and relevant.

Titles should be reflected as font size 26, and in bold type.

Ⅳ. Section Headings

Section headings, sub-headings, and sub-subheadings should be differentiated by font size.

Section Headings: Font size 22, bold type

Sub-Headings: Font size 16, bold type

Sub-Subheadings: Font size 14, bold type

Main Manuscript Outline

Ⅴ. Introduction

The introduction should highlight the significance of the research conducted, in particular, in relation to current state of research in the field. A clear research objective should be conveyed within a single sentence.

Ⅵ. Methodology/Methods

In this section, the methods used to obtain the results in the paper should be clearly elucidated. This allows readers to be able to replicate the study in the future. Authors should ensure that any references made to other research or experiments should be clearly cited.

Ⅶ. Results

In this section, the results of experiments conducted should be detailed. The results should not be discussed at length in

this section. Alternatively, Results and Discussion can also be combined to a single section.

Ⅷ. Discussion

In this section, the results of the experiments conducted can be discussed in detail. Authors should discuss the direct and indirect implications of their findings, and also discuss if the results obtain reflect the current state of research in the field. Applications for the research should be discussed in this section. Suggestions for future research can also be discussed in this section.

Ⅸ. Conclusion

This section offers closure for the paper. An effective conclusion will need to sum up the principal findings of the papers, and its implications for further research.

Ⅹ. References

References should be included as a separate page from the main manuscript. For parts of the manuscript that have referenced a particular source, a superscript (ie. [x]) should be included next to the referenced text.

[x] refers to the allocated number of the source under the Reference List (eg. [1], [2], [3])

In the References section, the corresponding source should be referenced as:

[x] Author(s). Article Title [Publication Type]. Journal Name, Vol. No., Issue No.: Page numbers. (DOI number)

Ⅺ. Glossary of Publication Type

J = Journal/Magazine

M = Monograph/Book

C = (Article) Collection

D = Dissertation/Thesis

P = Patent

S = Standards

N = Newspapers

R = Reports

Kindly note that the order of appearance of the referenced source should follow its order of appearance in the main manuscript.

Graphs, Figures, Tables, and Equations

Graphs, figures and tables should be labelled closely below it and aligned to the center. Each data presentation type should be labelled as Graph, Figure, or Table, and its sequence should be in running order, separate from each other.

Equations should be aligned to the left, and numbered with in running order with its number in parenthesis (aligned right).

Ⅻ. Others

Conflicts of interest, acknowledgements, and publication ethics should also be declared in the final version of the manuscript. Instructions have been provided as its counterpart under Cover Letter.

BILINGUAL PUBLISHING CO.
Pioneer of Global Academics Since 1984

Non-Metallic Material Science

Aims and Scope

Non-Metallic Material Science publishes original research papers, reviews, and notes that offers professional review and publication to freely disseminate research findings mainly in the areas of Polymeric Materials, Composites and Hybrid Materials, Inorganic and Carbon-based Materials. The Journal focuses on innovations of research methods at all stages and is committed to providing theoretical and practical experience for all those who are involved in these fields.

Non-Metallic Material Science aims to discover innovative methods, theories and studies in its field by publishing original articles, case studies and comprehensive reviews.

The scope of the papers in this journal includes, but is not limited to:

- Polymeric Materials
- Composites, Multi-component Materials and Hybrid Structures
- Inorganic and Carbon-based Materials
- Ceramics
- Dental Materials
- Semiconductor Materials
- Synthesis, Characterization, and Processing of Non-Metallic Materials
- Engineering Applications and Recycling of Non-Metallic Materials
- Modeling of Material Properties

Bilingual Publishing Co. (BPC)

Tel:+65 65881289

E-mail:contact@bilpublishing.com

Website:www.bilpublishing.com

About the Publisher

Bilingual Publishing Co. (BPC) is an international publisher of online, open access and scholarly peer-reviewed journals covering a wide range of academic disciplines including science, technology, medicine, engineering, education and social science. Reflecting the latest research from a broad sweep of subjects, our content is accessible world-wide——both in print and online.

BPC aims to provide an analytics as well as platform for information exchange and discussion that help organizations and professionals in advancing society for the betterment of mankind. BPC hopes to be indexed by well-known databases in order to expand its reach to the science community, and eventually grow to be a reputable publisher recognized by scholars and researchers around the world.

BPC adopts the Open Journal Systems, see on ojs.bilpublishing.com

Database Inclusion

Asia & Pacific Science Citation Index

Creative Commons

China National Knowledge Infrastructure

Google Scholar

Crossref

MyScienceWork

BILINGUAL
PUBLISHING CO.
Pioneer of Global Academics Since 1984

Tel:+65 65881289
E-mail:contact@bilpublishing.com
Website:www.bilpublishing.com

ISSN 2661-3301
02
9 772661 330208
Price: S$30.00